Science
AAAS

Supplementary Materials for

Mechanism of membrane-tethered mitochondrial protein synthesis

Yuzuru Itoh, Juni Andréll, Austin Choi, Uwe Richter, Priyanka Maiti, Robert B. Best, Antoni Barrientos, Brendan J. Battersby, Alexey Amunts

Correspondence to: abarrientos@med.miami.edu, brendan.battersby@helsinki.fi, amunts@scilifelab.se

This PDF file includes:

Other Supplementary Materials for this manuscript include the following:

Materials and Methods

Cell culture and isolation of mitochondria

HEK293-derived cells were grown in Freestyle 293 Expression Medium (Thermofisher 12338026) containing 5% tetracycline-free fetal bovine serum (FBS) in vented shaking flasks at 37 °C, 5% CO_2, and 120 rpm. Alternatively, cells were cultured in "Complete Medium" using high-glucose Dulbecco's modified Eagle's medium (Gibco # 11995-065,) supplemented with 10% FBS (Sigma # 12303C), 50 mg/ml uridine, 3 mM sodium formate, and 1x Penicillin-Streptomycin (ThermoFisher # 15070063) at 37 °C under 5% CO_2. Analysis of mycoplasma contamination was routinely performed.

For cryo-EM, the culture was scaled up sequentially by inoculating at 1.5 x 10^6 cells/ml and subsequently splitting at a cell density of 3.0 x 10^6 cells/ml up to a final volume of 2 L of cell culture. Actinonin (Sigma A6671) was added at the concentration of 65 μM directly to the cell suspension, and the cells were harvested after 3 hours with a density of 3.7 x 10^6 cells/ml by centrifugation at 1,000 g for 7 minutes, 4 °C. The pellet was washed and resuspended in 200 ml Phosphate Buffered Saline (PBS). The washed cells were pelleted at 1,000 g for 10 minutes at 4 °C. The resulting pellet was resuspended in 120 ml of MIB buffer (50 mM HEPES-KOH, pH 7.5, 10 mM KCl, 1.5 mM $MgCl_2$, 1 mM ethylenediaminetetraacetic acid (EDTA), 1 mM ethylene glycol-bis(β-aminoethyl ether) tetraacetic acid (EGTA), 1 mM dithiothreitol (DTT), protease inhibitors) and allowed to swell in the buffer for 15 minutes in the cold room by gentle stirring. About 45 ml of SM4 buffer (840 mM mannitol, 280 mM sucrose, 50 mM HEPES-KOH, pH 7.5, 10 mM KCl, 1.5 mM $MgCl_2$, 1 mM EDTA, 1 mM EGTA, 1 mM DTT, protease inhibitors) was added to the cells in MIB buffer and poured into a N_2 cavitation device kept on ice. The cells were then subjected to a pressure of 500 psi for 20 minutes before releasing the nitrogen from the chamber and collecting the lysate.

Mitochondria were isolated through differential centrifugation steps, followed by a sucrose gradient step (*33*). The lysate was clarified by centrifugation at 800 g and 4 °C for 15 minutes to separate the cell debris and nuclei. The supernatant was passed through a cheesecloth into a beaker kept on ice. The pellet was resuspended in half the previous volume of MIBSM buffer (3 volumes MIB buffer + 1 volume SM4 buffer) and homogenized with a Teflon/glass Dounce homogenizer. After clarification as described before, the resulting lysate was pooled with the previous batch of the lysate and subjected to centrifugation at 1,000 g, 4 °C for 15 minutes to ensure complete removal of cell debris. The clarified and filtered supernatant was centrifuged at 10,000 g and 4 °C for 15 minutes to pellet crude mitochondria. Crude mitochondria were resuspended in 10 ml MIBSM buffer and treated with 200 Units of RNase free DNase for 20 minutes in the cold room to remove contaminating genomic DNA. Crude mitochondria were again recovered by centrifugation at 10,000 g, 4 °C for 15 minutes and gently resuspended in 2 ml SEM buffer (250 mM sucrose, 20 mM HEPES-KOH, pH 7.5, 1 mM EDTA). Resuspended mitochondria were subjected to a sucrose density step-gradient (1.5 ml of 60% sucrose; 4 ml of the 32% sucrose; 1.5 ml of 23% sucrose and 1.5 ml of 15% sucrose in 20 mM HEPES-KOH, pH 7.5, 1 mM EDTA), centrifugation in a Beckmann Coulter SW40 rotor at 140,000 g for 60 minutes. Mitochondria seen as a brown band at the interface between the 32% and 60% sucrose layers was collected and flash-frozen using liquid nitrogen and transferred to −80 °C.

T-Rex inducible expression system

For biochemical studies, a T-Rex inducible expression system was used, which functions by the binding of tetracycline (tet) to a tet-repressor protein causing its dissociation from a tet-

operon adjacent to the gene of interest promoter. Dissociation of the tet-repressor allows for overexpression of the gene of interest. The system consists of two plasmids: pcDNA6/TR that expresses the tet-repressor protein and pcDNA6/TO/Myc-His (Thermo Fisher # V22120), which expresses the gene of interest under the control of the tet-operator. We obtained the T-Rex 293 cell line (Thermo Fisher Scientific # R71007), which stably expresses the tet-repressor protein from the pcDNA6/TR plasmid. T-Rex293 was then stably transfected with modified *mL45* constructs in the pcDNA6/TO/myc-His plasmid. Overexpression of mL45 from pcDNA6/TO/myc-His in T-Rex293 was induced by the addition of 10 ng/ml doxycycline.

RNAi Silencing

Silencing of endogenous *mL45* was achieved through transient transfection of *mL45* targeting short interfering RNA (si-*mL45*) for 6 days. In detail, for a single well of a 6-well plate, T-Rex293 was seeded with the number of cells allowing three days of growth before reaching 80-90% confluency (~$1.5x10^5$ cells) in 2 ml complete media. Three hours after seeding, silencing treatment began by the addition of silencing media. Silencing media is a mixture of two solutions, "A" and "B". Solution A contains 100 µL Opti-MEM (ThermoFisher # 31985062) and 2.5 µL RNAiMax (Invitrogen # 13778030). Solution B contains 100 µL Opti-MEM and 2 µL 20 µM si-*mL45* (Invitrogen Cat # 4392420, ID # s38889) or non-targeting siRNA (Invitrogen # 4390843). Solutions A and B were made separately, then mixed to form the silencing media and incubated at room temperature for 10 minutes. Silencing media was then added dropwise to the culture well. Cells were then allowed to grow under normal culture conditions for three days. After three days of treatment, cells approached 90% confluency and were split and reseeded, and silencing treatment was resumed by the addition of fresh silencing media three hours later. Cells were then cultured for an additional three days before collection and analysis. For experiments requiring greater cell numbers, cells were seeded in larger culture vessels for which the volume of reagents in silencing media was adjusted according to the Lipofectamine® RNAiMAX Reagent Protocol. Optimal cell seeding density was individually determined for each culture vessel.

Construction and transfection of ΔN-*mL45*

To generate a ΔN-*mL45* construct that is not targeted by si-*mL45*, we designed a synthetic *mL45* coding sequence (CDS) such that each codon contains silent mutations, which prevent recognition by si-*mL45* but encode a protein identical to endogenous mL45 hereby referred to as optimized *mL45(mL45-Opti)*. *mL45-Opti* was designed using the IDT (Integrated DNA Technologies) Codon Optimization Tool and ordered as a double-stranded DNA fragment. *mL45-Opti* was then cloned into the pcDNA6/myc-6xHis vector using the In-Fusion® HD Cloning Plus kit (Takara # 638911). A C-terminal FLAG tag (DYKDDDDK) was added to the *mL45-Opti* CDS immediately before the stop codon. Deletion of the mL45 N-terminal (ΔN=I45-R74) was then made in the *mL45-Opti* construct using the Q5® Site-Directed Mutagenesis Kit (New England Biolabs # E0554S) (Construct name: ΔN-mL45). ΔN-mL45 was then transfected into the T-Rex293 cell line (Thermo Fisher Scientific # R71007) by lipofection with EndoFectin Max (GeneCopoeia # EF013) as per manufacturer instructions in a 6-well plate with 1.5 µg plasmid DNA for 24 hours. Growth media was then replaced, and 500 µg/ml Zeocin (Gibco # R25001) was added to select cells stably expressing ΔN-mL45. After two weeks of selection, ΔN-mL45 construct or empty vector expressing stable pools were collected and stored in

freezing media (complete media supplemented with 30% FBS & 5% DMSO) and frozen in liquid nitrogen for later use.

Expression of ΔN-mL45 and co-immunoprecipitation

To examine the consequence of *mL45* N-terminal deletion, T-Rex293 cells stably expressing *mL45*-ΔN were treated with si-*mL45* for six days, at which point endogenous mL45 is not detectable by immunoblot. The steady-state levels of *mL45*-ΔN were approximately 25% of the WT. Mitochondria were isolated for use in co-immunoprecipitation studies.

All steps the subsewuent steps were conducted at 4°C. 1 mg of isolated mitochondria was lysed in 285 µL of co-IP general buffer (10 mM potassium acetate, 5 mM magnesium acetate, 0.8 mM EDTA, 5 mM β-mercaptoethanol, 1 mM phenylmethylsulfonyl fluoride, 1x Roche protease inhibitor (Millipore Sigma #11697498001), 10 mM pH 7.4 Tris-HCl, and 5% glycerol) with 0.5% n-Dodecyl β-D-maltoside (DDM) for 10 min on ice. The lysis was ended by the addition of 570 µL of co-IP general buffer without DDM. The lysate was cleared for 5 min at 15,000 x g. The supernatant was then split into two aliquots. 50 µL of each aliquot was set aside as ("Total" fraction) for later analysis. Each aliquot was then combined with 50 µL protein A conjugated agarose beads (Thermo Fischer #20365) coated with either α-mL45 (Thermo Fischer PA5-54784) or rabbit IgG (Millipore Sigma 12-370) then adjusted to a final volume of 500 µL by adding co-IP general buffer. Samples were incubated on a rotator for 4 hours. Beads were then isolated at 200 x g. The supernatant of each sample was collected as "Unbound" fraction. Beads were gently washed 4 times by resuspension in co-IP general buffer + 0.05% DDM followed by re-isolation of beads by centrifugation at 200 x g. Bound proteins were eluted from beads by the addition of 50 µL of 4x Laemmli sample buffer (250 mM Tris HCl, 8% SDS, 40% Glycerol, 0.02% Bromophenol blue, 8% ß-mercaptoethanol) to collect "IP" fraction. 16.5 µL of 4x Laemmli sample buffer was added to 50 µL of Total and Unbound samples and were analyzed by SDS-PAGE.

SDS-PAGE and immunoblotting

To estimate the steady-state levels of specific proteins of interest, whole-cell protein extracts (WCE) were analyzed by denaturing SDS-PAGE and immunoblotting. Total cellular proteins were extracted in RIPA buffer (1% NP-40, 0.1% SDS, 0.5% Na deoxycholate, 150 mM NaCl, 2 mM EDTA, and 50 mM Tris-HCl, pH 8.0) with freshly added 1 mM PMSF and 1X EDTA-free protease inhibitor cocktail (Roche). Protein concentration in WCE and mitochondrial preparations was measured with the Folin phenol reagent (*34*). In general, 40-60 µg of WCE were separated by SDS-PAGE in the Laemmli buffer system (*35*). After transfer to a nitrocellulose membrane, the membranes with immobilized proteins were blocked with 2.5% skim milk and then incubated with antibodies against the indicated proteins followed by a second reaction with anti-mouse or anti-rabbit IgG conjugated to horseradish peroxidase. β-ACTIN was used as a loading control. Signals were detected by chemiluminescence incubation and X-ray film. Optical densities of the immunoreactive bands were measured using the ImageLab (Biorad) software or the ImageJ software in digitalized images. The list of antibodies used in this study is included in the supplementary material Table S5.

Pulse Labeling of Mitochondrial Translation Products

Mitochondrial protein synthesis was determined by pulse-labeling 70-80% confluent T-Rex293 cultures in the presence of inhibitors of cytoplasmic protein synthesis. The irreversible

inhibitor emetine was used to prevent translation from cytosolic ribosomes (*36*). Cells were labeled for 30 min (Pulse) at 37 °C with 150 μCi/ml [^{35}S] methionine (PerkinElmer Life Sciences, Boston, MA). After incubation, the cells were washed once with 1X PBS, collected by trypsinization, and whole-cell extracts were prepared by solubilization in RIPA buffer (1% NP-40, 0.1% SDS, 0.5% Na-deoxycholate, 150 mM NaCl, 2 mM EDTA (ethylenediaminetetraacetic acid), and 50 mM Tris-HCl, pH 8.0) supplemented with 1 mM PMSF (phenylmethylsulfonyl fluoride) and 1X EDTA-free mammalian protease inhibitor cocktail (Roche # 11836170001). After incubation, the cells were washed, trypsinized, collected, and proteins were extracted. 100 ug of each sample were separated by SDS (sodium dodecyl sulfate)-PAGE on a 17.5% polyacrylamide gel, transferred to a nitrocellulose membrane, and exposed to Kodak X-OMAT X-ray film. The membranes were then probed with a primary antibody against β-ACTIN as a loading control.

For erythromycin treatment experiments, cells were treated for 4 hours with indicated doses of erythromycin. A similar concentration of DMSO was used as control. Cells were labeled with ^{35}S-methionine for 30 min (Pulse) in the presence or absence of erythromycin (since erythromycin is a reversible inhibitor), and proteins were extracted as described above.

Membrane flotation analysis of mL45

Soluble and membrane-associated or embedded proteins were separated by flotation gradient centrifugation, as previously described (*31*). In detail, purified mitochondria were suspended in 50 mM KCl, 10 mM $MgCl_2$, 20 mM Tris/HCl, pH7.4, 1 mM PMSF and disrupted by 3 x 30 s sonication in an ultrasonic cleaner bath (Sper Scientific 100004), with 1 minute of cooling on ice, then three freeze-thawing cycles of 5 minutes at −80 °C and 20-minute thaw on ice. The sample (see fig. S10 “Input”) was then adjusted to final 1.6 M sucrose in 300 μl, loaded into a centrifugation tube, and layered with 250 μl 1.4 M sucrose and 100 μl 0.25 M sucrose on top. Sucrose solutions were prepared in the same buffer used to resuspend mitochondria. The samples were centrifuged in a Beckman SW55Ti rotor for 4.5 h at 255,000 g at 4 °C, and the gradient was split into membrane (top half - M) and soluble (bottom half, S) fractions. An equal volume of each fraction was loaded on an SDS-PAGE gel and analyzed by immunoblotting. An input sample was included as a control. Immunoblot against LETM1 (integral membrane protein) and HSP10 (soluble matrix protein) were used to confirm successful fractionation.

Purification of mitoribosomes for cryo-EM

Mitochondria thawed on ice were solubilized in lysis buffer (25 mM HEPES-KOH pH 7.5, 20 mM KCl, 20 mM $Mg(OAc)_2$, 2 mM DTT, protease inhibitors, 25 μM actinonin, 1 mM ATP, and 2% n-dodecyl-β-D-maltoside (β-DDM)). The suspension was incubated on a roller in the cold room for 30 min. A small Teflon/glass Dounce homogenizer was used to homogenize mitochondria for efficient lysis. After incubation on ice for 5-10 minutes, the lysate was clarified by centrifugation at 30,000 g for 20 minutes, 4 °C. The clarified lysate was carefully collected. Centrifugation was repeated to ensure complete clarification. The mitochondrial lysate was loaded onto 0.4 ml sucrose cushion (34% sucrose, 25 mM HEPES-KOH pH 7.5, 20 mM KCl, 20 mM $Mg(OAc)_2$, 2 mM DTT, 25 μm actinonin, 1 mM ATP and 1% DDM). Centrifugation was carried out at 233,000 g for 45 minutes in a TLA120.2 rotor. The supernatant was discarded, and the pellets washed and resuspended in resuspension buffer (25 mM HEPES-KOH pH 7.5, 40 mM KCl, 10 mM $Mg(OAc)_2$, 2mM DTT, 0.02% DDM). Pooled fractions were gently vortexed and centrifuged at 13,000 g for 10 min. Centrifugation was repeated to ensure complete

clarification. The supernatant was applied on to a linear 15-30% sucrose gradient (20 mM HEPES-KOH, pH 7.5, 40 mM KCl, 10 mM $Mg(OAc)_2$, 0.02 % β-DDM, 2 mM DTT) and centrifuged in a TLS55 rotor at 214,000 g for 120 minutes. The gradient was fractionated by piercing the bottom of the gradient tube with a PrecisionGlide Needle (BD) and collecting the ~50 µl aliquots. The absorbance at A_{260} was measured, and the fractions corresponding to the latter half of the monosome peak were pooled and buffer exchanged into resuspension buffer using a 100 kDa cutoff vivaspin concentrator (Sartorius VS0142). The sample was concentrated to A_{260} value of 4.2, and grids were immediately prepared.

For crosslinking, 1 mM BS3 crosslinker (Thermofisher A39266) was added to the purified mitoribosomes from the sucrose cushion step and incubated for 60 min on ice. BS3 is a water-soluble crosslinker with 11 Å spacer, which irreversibly links two amino groups such as those of lysine sidechains and N-terminal residues. The reaction was quenched for 10 min at room temperature with 50 mM ammonium bicarbonate prior to loading the sample onto the sucrose gradient.

Mass spectrometry analysis

The samples for mass spectrometry analysis were prepared to identify the non-ribosomal membrane proteins associated with the translating mitoribosome. The complex was purified exactly as for the cryo-EM analysis. The gradient was fractionated, and the monosome peak was collected. The pooled fractions were subjected to buffer exchange with the resuspension buffer to dilute away sucrose. The purified solution was submitted for mass spectrometry analysis.

The purified samples were lysed by 4% SDS lysis buffer and prepared for mass spectrometry analysis using a modified version of the solid phase-enhanced sample-preparation (SP3) protein clean up and digestion protocol (*37*). In brief, 33 and 22 µg protein from each sample was alkylated with 4 mM Chloroacetamide. Sera-Mag SP3 bead mix (20 µl) was transferred into the protein sample together with 100% acetonitrile to a final concentration of 70 %. The mix was incubated under rotation at room temperature for 18 min. The mix was placed on the magnetic rack, and the supernatant was discarded, followed by two washes with 70 % ethanol and one with 100 % acetonitrile. The beads-protein mixture was reconstituted in 100 µl LysC buffer (0.5 M Urea, 50 mM HEPES pH 7.6, and 1:50 enzyme (Trypsin) to protein ratio) and incubated overnight. Finally, the peptide samples were desalted by strong cation-exchange chromatography (SCX) clean up. The final peptide concentration was determined by the Bio-Rad DC Assay. An aliquot of approximately 10 µg was suspended in LC mobile phase A, and 3 µg was injected into the LC-MS/MS system.

Online LC-MS was performed using a Dionex UltiMate™ 3000 RSLCnano System coupled to a Q-Exactive High Field mass spectrometer (Thermo Scientific). 3 uL was injected from each sample. Samples were trapped on a C18 guard desalting column (Acclaim PepMap 100, 75µm x 2 cm, nanoViper, C18, 5 µm, 100 Å), and separated on a 50 cm long C18 column (Easy spray PepMap RSLC, C18, 2 µm, 100 Å, 75 µm x 50cm). The nanocapillary solvent A was 95% water, 5% DMSO, 0.1% formic acid, and solvent B was 5% water, 5% DMSO, 95% acetonitrile, 0.1% formic acid. At a constant flow of 0.25 µl min^{-1}, the curved gradient went from 6% B up to 43% B in 180 min, followed by a steep increase to 100% B in 5 min. Fourier Transform Mass Spectrometry (FTMS) master scans with 60,000 resolution (and mass range 300-1500 m/z) were followed by data-dependent MS/MS (30,000 resolution) on the top 5 ions using higher energy collision dissociation (HCD) at 30% normalized collision energy. Precursors were isolated with a 1.2 m/z window. Automatic gain control (AGC) targets were 1e6 for MS1 and 1e5 for MS2.

Maximum injection times were 100 ms for MS1 and MS2. The entire duty cycle lasted ~2.5 sec. Dynamic exclusion was used with 60 sec duration. Precursors with unassigned charge state or charge state 1 were excluded. An underfill ratio of 1% was used.

The MS raw files were searched using Sequest-Percolator or Target Decoy PSM Validator under the software platform Proteome Discoverer 1.4 (Thermo Scientific) against *Homo sapiens* Uniprot database and filtered to a 1% false discovery rate (FDR) cut off. We used a precursor ion mass tolerance of 10 ppm, and product ion mass tolerances of 0.02 Da for higher energy collision dissociation Fourier Transform Mass Spectrometry (HCD-FTMS). The algorithm considered tryptic peptides with maximum 2 missed cleavage; carbamidomethylation (C) as fixed modification, and oxidation (M) as variable modifications.

Preparation of cryo-EM grids and data collection

R2/2 300 mesh copper grids (Quantifoil) with a nominal 3 nm carbon support layer (produced in a Quorum Q150T) were glow-discharged (20 mA 30 sec on a PELCO easiGlow apparatus) immediately prior to use. A 3 µl sample was applied onto the grid in a Vitrobot Mark IV robot (FEI Thermofisher) (4 °C, 100% humidity, blot force of 0, blot time of 3 sec, standard Vitrobot filter paper grade 595) and plunge-frozen into liquid ethane. Data were collected on eight separate occasions on a Titan Krios (FEI ThermoFisher) operated at 300 kV with a Quantum K2 summit detector (Gatan) using EPU software (FEI Thermofisher) at a pixel size of 0.83 Å. Datasets 1-6 were collected on grids from native preparations. Datasets 7-8 were collected on grids from the crosslinked preparation. Datasets 1 and 3-6 were collected on the same grid, and dataset 2 was collected on a copy grid from the same purification. Datasets 7 and 8 were collected from two copy grids from the same purification of crosslinked mitoribosomes. For all datasets, movies with 20 frames were collected with a dose rate of 5.0-5.7 electrons per pixel per second with an exposure time of 4 seconds and a total dose of 29-32 electrons per $Å^2$.

Image processing

The movies were gain corrected, dose weighted, and aligned with Motioncor2 (*38*) and the contrast transfer function (CTF) estimated using gctf (*39*). Micrographs with sensible CTF estimations in the defocus range of -0.2 to -3.6 µm were kept. Particles were picked with RELION-3.0 (*15*) (datasets 1-2) or Warp (*40*) (datasets 3-6). Subsequent processing steps were performed in RELION-3.0. The particles were 2D classified separately (datasets 3 and 4) or together (datasets 1-2 and datasets 5-6) depending on how close in time they were collected. After 2D classification, the selected particles were refined in four separate groups (datasets 1-2, dataset 3, dataset 4, datasets 5-6). Refined particles from datasets 1-2, 3, and 4 were 3D classified separately for cleaning purposes, and the classes containing mtLSU and monosome particles from each group were kept and pooled into a combined total of 1,392,976 particles. These particles (3x binned) were refined together, and partial signal subtraction and masked 3D classification with alignment on the mtSSU were performed. 797,737 particles (1.5x binned) containing mtSSU were selected from datasets 1-4 and refined. Partial signal subtraction and masked 3D classification (with alignment) on the mtSSU was carried out on refined particles from datasets 5-6. This one step was sufficient to both clean the data and select 429,443 monosome particles. The two sets of particles from datasets 1-4 and datasets 5-6 were pooled into 1,227,180 monosome particles (1.5x binned) and refined together with a mask on the mtLSU. Partial signal subtraction and masked 3D classification (no alignment) on the A site tRNA isolated 456,527 particles, which were refined with a mask on the mtLSU. A final partial

signal subtraction and masked 3D classification (no alignment) on the insertase density near mL45 yielded 91,244 particles (unbinned) that refined to 3.39 Å with a mask on the mtLSU.

For the crosslinked data, the movies were processed in the same manner as those for non-crosslinked data. Particles were picked with Warp (*40*), and subsequent processing steps were performed in RELION3.0 (*15*). Selected particles (3x binned) after 2D classification were refined, and partial signal subtraction and masked 3D classification with alignment on the mtSSU were carried out. 241,399 selected particles (1.5x binned) were refined to 2.95 Å with a mask on the mtLSU. In the initial processing round, partial signal subtraction and masked 3D classification (no alignment) on the A-site tRNA isolated 138,524 particles, which were refined with a mask on the mtLSU. A final partial signal subtraction and masked 3D classification on the insertase region near mL45 yielded 30,744 particles with density in the insertase region (Class 1a) and 93,615 particles without this density (Class 1b). The unbinned particles from each class refined with a mtLSU mask to 3.20 Å and 2.99 Å resolution, respectively.

After comparison with the map from the native data, the crosslinked data were selected for further processing. To improve resolution, CTF refinement and Bayesian particle polishing were attempted. Hence the movies from datasets 7-8 were motion-corrected in RELION-3.0 (*15*), and unbinned 241,399 monosome particles were subjected to CTF refinement (per-particle defocus), followed by a Bayesian particle polishing and the second round of CTF refinement (per-particle defocus and astigmatism and beam tilt). From these monosome particles, the identical sets of particles in the initial processing round (Class1a*: 30,744 particles, Class 1b*: 93,615 particles) were extracted and refined with a mtLSU-body mask, resulting in 2.89 Å and 2.59 Å resolution, respectively (fig. S2B). Local resolutions are shown in fig. S5. To improve local resolution of other areas, mask refinements were performed using four local masks, CP, L10-L7/L12-stalk, mtSSU-head, and mtSSU-body, respectively, fig. S2E-F. All maps were subjected to *B*-factor sharpening and local resolution filtering by RELION-3.0 (*15*). Data collection and processing statistics of the crosslinked data are given in Table S1.

Model building and refinement

Model building of Class1a* (OXA1L-bound) and Class 1b* (without OXA1L) from the crosslinked data were performed. The structures of human mitoribosome PDB IDs 3J9M (*25*) and 5OOL (*27*), and 6RW4 (*41*) were used as starting models against the cryo-EM density maps and manually adjusted in *Coot* (*42*) with Ramachandran restraints. The consensus parts of the two classes were modeled first. A- and P-site tRNAs and mRNA were modeled *de novo* in the density. Since bound tRNAs and mRNAs are a mixture of any mitochondrial ones, each residue was assigned as either A, U, G, or C, based on the density and conservation. Ligands, metal ions, water molecules, and modifications were placed into the density. Differences between two classes were then listed up by comparing their maps and introduced into the model. These are located around the OXA1L contact sites and the peptide tunnel, including uL23m, uL24m, mL45, and rRNA H50.

In Class1a*, the entire rRNAs except for the L1-stalk were modeled, while uL23m residues 114-132 and mL45 residues 96-108 and 202-205 were not modeled due to the disordered density. The N-terminal tail of mL45 was traced through the density in the cavity of the peptide exit, and *de novo* model building was conducted based on the defined densities. Since a natively-purified nascent polypeptide represents a mixture of sequences, 32 residues resolved residues were modeled as a poly-alanine chain in the density inside the tunnel, connected to the 3′-terminus of the P-site tRNA. During rRNA model adjustment, extra density corresponding to a

short helix was found at site 1. Based on the clear sidechain densities, the OXA1L C-terminal sequence YPWHDTLG was placed unambiguously, and three residues were added toward site 2 in the less clear density. Forty residues of OXA1L-CTE were modeled *de novo* in the tube-shaped extra density at site 2. Since the density alone is not clear enough for unambiguous sidechain assignment, the information of the secondary structure predicted by PSIPRED (*43*) and the neighboring uL24m residues were also considered. In Class1b*, the three unmodeled regions in uL23m and mL45 were modeled, while the residues 2357-2359 in rRNA H50 were not modeled due to the unclear density. The N-terminal tail of mL45 was traced into the peptide tunnel instead of the nascent polypeptide. The information on built proteins is in the Tables S2-4.

Hydrogens were generated to have better clash scores, and stereochemical and *B*-factor refinements were performed using phenix.real_space_refine in the PHENIX suite (*44*). Reference restrains were used for the protein parts with sigma 2, using the input model as the reference. No rotameric or Ramachandran restraints were used. The local-masked refined maps with sharpening and local-resolution filtering were combined and used as the target for model refinement. The final models were validated using MolProbity (*45*). Refinement statistics are given in Table S1. The path and diameter of the nascent polypeptide tunnel are detected by CAVER 3.0 (*46*). Figures were generated using PyMOL (*47*), UCSF Chimera (*48*), and UCSF ChimeraX (*49*). Ribosomal proteins are named following the recently adopted nomenclature (*50*).

Image quantification, statistical analysis, and sequence alignment

All experiments were done with three or more biological replicates unless otherwise indicated. Data in X-ray films were digitized and analyzed using the Image J software. The data quantification in Fig. 2 is presented as the mean proportion of mL45 detected as the percentage of total mL45 loaded.

Sequence alignments were done in Jalview (*51*) using Clustal WS (*52*) and Clustal O (*53*). The following vertebrate sequences were used: *Homo sapiens*, *Mus musculus*, *Xenopus tropicalis*, *Danio rerio.* The following bacterial sequences were used: *Escherichia coli*, *Staphylococcus aureus*, *Synechococcaceae cyanobacterium, Thermus thermophilus*.

Coarse-grained molecular simulations

Coarse-grained simulations were performed to ascertain the effect of the constriction caused by mL45 in the OXA1L bound structure. Initial structures were taken from the all-atom model of the OXA1L-bound complex. For regions of proteins which were missing, owing to disorder, the residues were initially included based on the corresponding region in the inactive structure (in which they were present) Specifically, these regions were residues 114-132 of uL23m and residues 96-108 and 202-205 of mL45. For the nascent chain, 45 residues were added to the N-terminus to address the requirements for helix formation. Each protein residue was represented by a single bead centered on the C_α carbon atom, while each RNA residue was represented by three beads, one each for the ribose, phosphate and nucleobase centered respectively at the C4′, P and N3 atoms of each residue. The interactions were represented by a coarse-grained energy function

$$E = \sum_{(i,j)\in\text{bonds}} \frac{1}{2}k_b\left(r_{ij} - r_{ij,0}\right)^2 + \sum_{(i,j,k)\in\text{angles}} \frac{1}{2}k_a\left(\theta_{ijk} - \theta_{ijk,0}\right)^2 + \sum_{(i,j)\notin\text{Native}} 4\varepsilon_{ij}\left(\left(\frac{\sigma_{ij}}{r_{ij}}\right)^{12} - \left(\frac{\sigma_{ij}}{r_{ij}}\right)^{6}\right) + \sum_{(i,j)\in\text{Native}} 4\hat{\varepsilon}_{ij}\left(\left(\frac{\hat{\sigma}_{ij}}{r_{ij}}\right)^{12} - \left(\frac{\hat{\sigma}_{ij}}{r_{ij}}\right)^{6}\right) + \sum_{i,j} \frac{q_i q_j}{4\pi\epsilon_0 D r_{ij}} \exp\left[-\frac{r_{ij}}{\lambda_{\text{DH}}}\right] \quad (1)$$

The first two terms of eq. 1 account for the covalently bonded structure of the chain, with r_{ij} the distance between atoms *i* and *j*, k_b the harmonic bond force constant, θ_{ijk} the angle between bonded atoms *i*, *j*, and *k*, and k_θ is the harmonic angle force constant. The ideal values of the bond lengths and angles ($r_{ij,0}$ and $\theta_{ijk,0}$ respectively) and the force constants as previously described (*54*). The third term of eq. 1 refers to a generic non-bonded term with parameters (*54*). The fourth term defines a structure-based term defining native structure formation, which was used to add specific 1,4 and 1,3 contacts favoring helix formation to the 56 N-terminal residues of the nascent chain, in which $\hat{\sigma}_{ij}$=5.5 Å and $\hat{\varepsilon}_{ij}$=8 kJ/mol for 1,4 contacts and $\hat{\sigma}_{ij}$=4.45 Å and $\hat{\varepsilon}_{ij}$=8 kJ/mol for 1,3 contacts. The last term is the Coulomb potential: every bead representing a charged amino acid in the mitoribosomal proteins is assigned the appropriate net charge (q_i) and the RNA phosphate beads are each given a charge of -1. Electrostatic forces are modified by a Debye-Hückel screening function with Debye length λ_{DH}=10 Å. The parameters ϵ_0 and *D* are respectively the permittivity of free space and the relative dielectric of the medium, taken to be 80.

This initial configuration was then energy minimized by steepest descents for 2000 steps to relieve clashes before starting the simulations. Simulations were run using Gromacs 2019.4 (*55*) with Langevin dynamics with a friction coefficient of 0.2 ps^{-1} and a time step of 10 fs. Most of the system was kept frozen and dynamics was only propagated for the nascent chain and regions of the ribosomal proteins that were disordered in the cryo-EM structure.

The fraction helix for residue *i* was determined by counting the fraction of saved snapshots in which the *i,i+4* distance was less than 7.5 Å (other definitions of helix formation did not qualitatively alter the results). Statistical errors were determined by block error analysis using 10 blocks (*56*).

Models of ribosomes and insertase with respect to the tunnel and the membrane

To model the human mitoribosome with the OXA1L insertase (fig. S15A), we used the X-ray crystal structure of YidC (PDB ID: 3WO6 (*57*)) as the template for the homology modeling for the membrane domain of OXA1L. The obtained model of OXA1L was then superimposed with the C-terminal part resolved in our study that is associated with the mitoribosome. The resulted model of the mitoribosome:OXA1L complex was placed in the context of the membrane, based on the fitting into the electron cryo-tomography map of *in situ* human mitoribosomes (EMD-3784 (*4*)). Finally, the membrane plane was shown with a lipid-like model obtained and modified from (*58*).

To model the *E. coli* ribosome with the YidC insertase (fig. S15B), we used the cryo-EM map of the ribosome:YidC complex (EMD-4155 (*17*)) to fit the model of the *E. coli* ribosome with mRNA and peptidyl-tRNA (PDB ID: 3JBU (*59*)), and YidC X-ray crystal structure (PDB

ID: 3WO6 (*57*)). The nascent chain was elongated by five residues to indicate the tunnel path. The distance between the ribosomes and the membrane surface was measured using a conserved region of uL24m as a reference point. The 4-fold difference reflects more flexible and distal association of the mitoribosome with OXA1L.

For the comparison of the tunnel diameters, shown in Fig. 4D, the *E. coli* ribosome PDB ID: 4YBB (*60*) was used. The diameter (>12 Å) of a helical formation within the tunnel was calculated from the reported experimental data (*61*). Also, the position of a folded helix was derived from the experimental data showing that nascent chains to begin folding in the exit tunnel (*29*). Together, this information was plotted along the tunnel path and compared with the mitoribosomal diameter calculated directly from the structure between the mL45 residues Pro48-mL45:Phe56-mL45:Arg33-uL24m (constriction 1) and Glu53-mL45:Glu70-mL45 (constriction 2). The comparison suggests that the enclosure of the nascent chain eliminates it from sampling an α-helical formation.

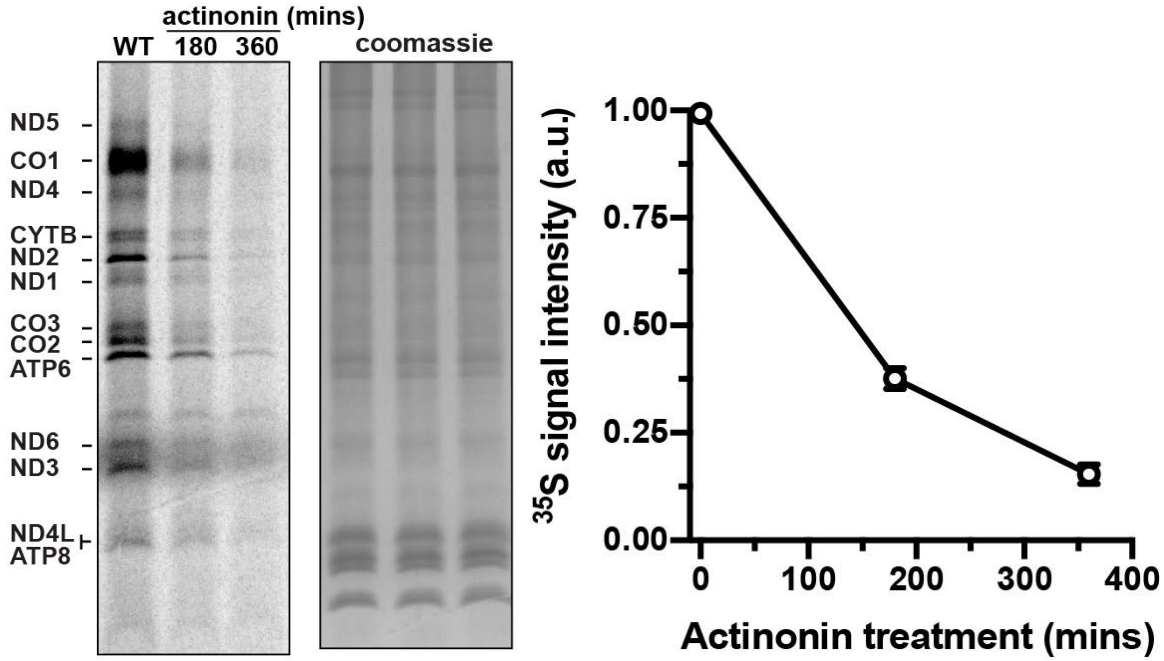

Fig. S1. Actinonin treatment of the cell prior preparation of mitochondria.

Actinonin-treated cells labelled with a pulse of ^{35}S-methionine/cysteine show inhibition of mitochondrial protein synthesis. Bottom: quantification of metabolic labelling, mean +/- standard deviation from three independent experiments.

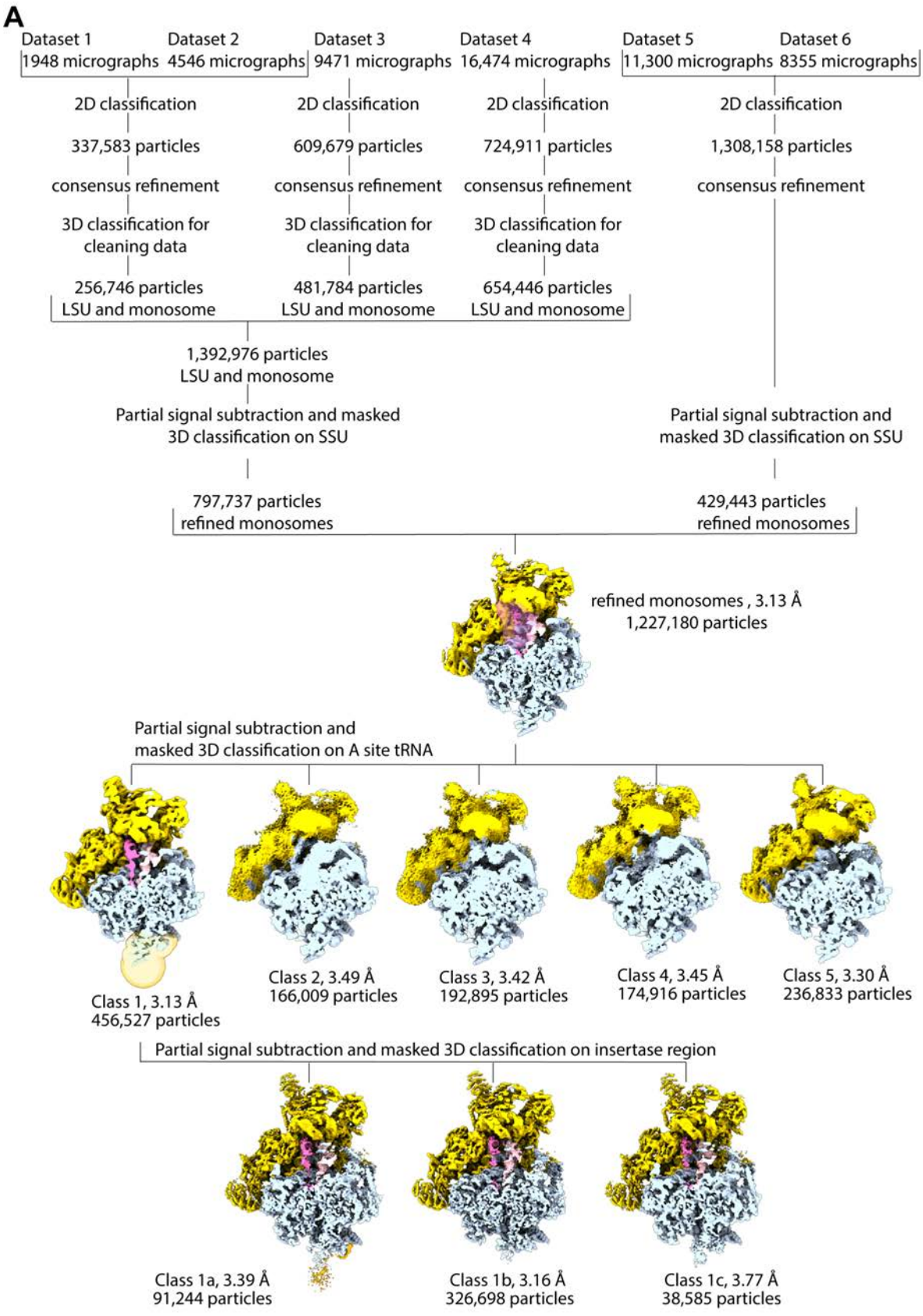
A
Dataset 1
1948 micrographs
Dataset 2
4546 micrographs
Dataset 3
9471 micrographs
Dataset 4
16,474 micrographs
Dataset 5
11,300 micrographs
Dataset 6
8355 micrographs
2D classification
337,583 particles
consensus refinement
3D classification for cleaning data
256,746 particles
LSU and monosome
2D classification
609,679 particles
consensus refinement
3D classification for cleaning data
481,784 particles
LSU and monosome
2D classification
724,911 particles
consensus refinement
3D classification for cleaning data
654,446 particles
LSU and monosome
2D classification
1,308,158 particles
consensus refinement
1,392,976 particles
LSU and monosome
Partial signal subtraction and masked 3D classification on SSU
Partial signal subtraction and masked 3D classification on SSU
797,737 particles
refined monosomes
429,443 particles
refined monosomes
refined monosomes , 3.13 Å
1,227,180 particles
Partial signal subtraction and masked 3D classification on A site tRNA
Class 1, 3.13 Å
456,527 particles
Class 2, 3.49 Å
166,009 particles
Class 3, 3.42 Å
192,895 particles
Class 4, 3.45 Å
174,916 particles
Class 5, 3.30 Å
236,833 particles
Partial signal subtraction and masked 3D classification on insertase region
Class 1a, 3.39 Å
91,244 particles
Class 1b, 3.16 Å
326,698 particles
Class 1c, 3.77 Å
38,585 particles

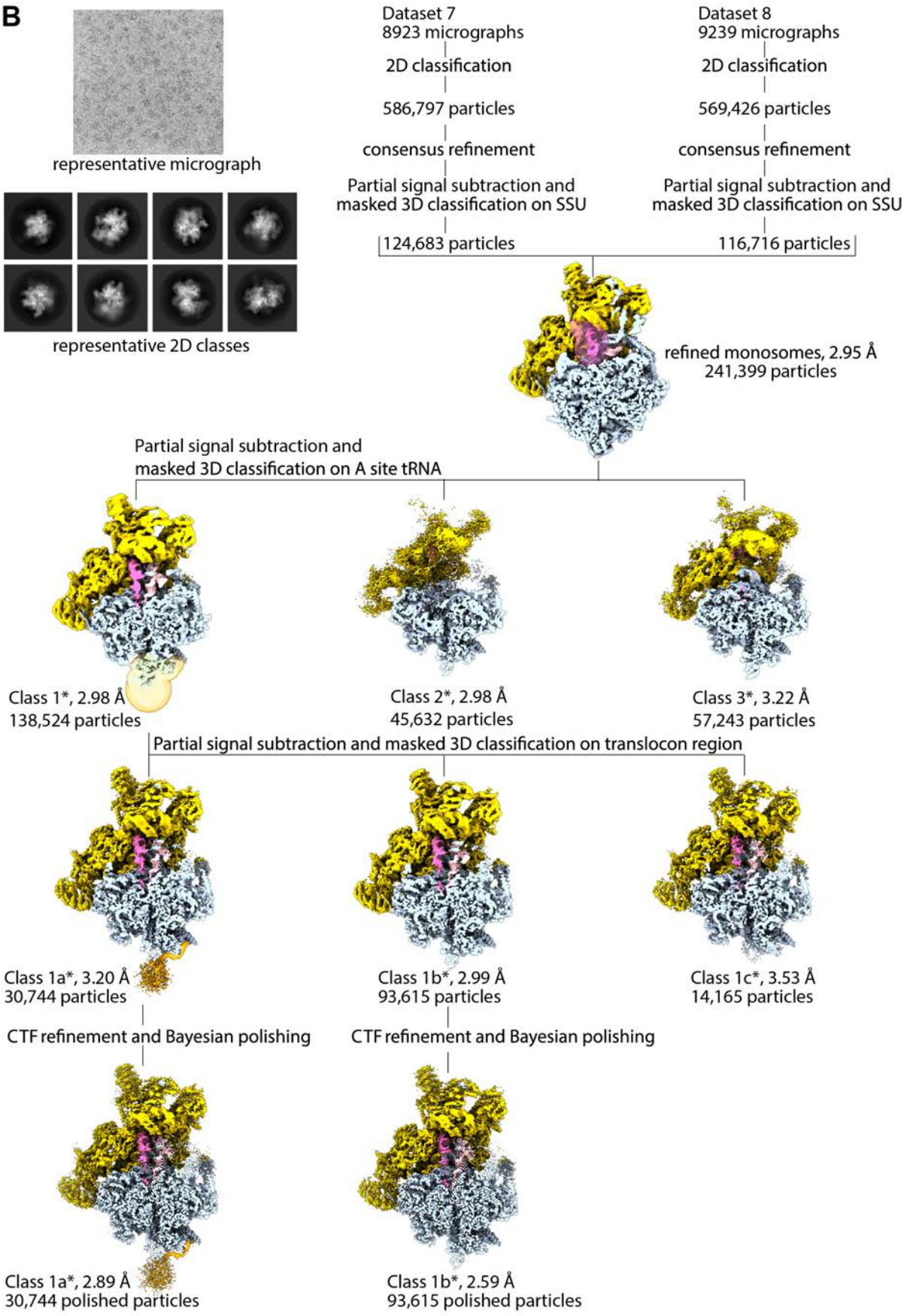
B
representative micrograph
representative 2D classes
Dataset 7
8923 micrographs
2D classification
586,797 particles
consensus refinement
Partial signal subtraction and
masked 3D classification on SSU
124,683 particles
Dataset 8
9239 micrographs
2D classification
569,426 particles
consensus refinement
Partial signal subtraction and
masked 3D classification on SSU
116,716 particles
refined monosomes, 2.95 Å
241,399 particles
Partial signal subtraction and
masked 3D classification on A site tRNA
Class 1*, 2.98 Å
138,524 particles
Class 2*, 2.98 Å
45,632 particles
Class 3*, 3.22 Å
57,243 particles
Partial signal subtraction and masked 3D classification on translocon region
Class 1a*, 3.20 Å
30,744 particles
Class 1b*, 2.99 Å
93,615 particles
Class 1c*, 3.53 Å
14,165 particles
CTF refinement and Bayesian polishing
CTF refinement and Bayesian polishing
Class 1a*, 2.89 Å
30,744 polished particles
Class 1b*, 2.59 Å
93,615 polished particles

C

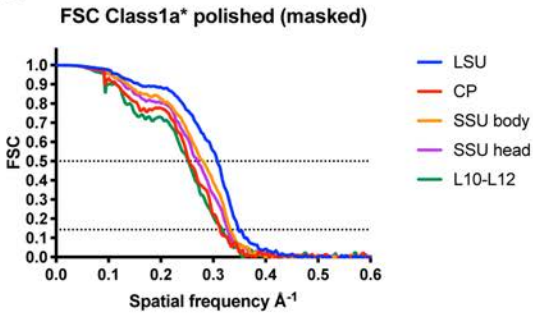

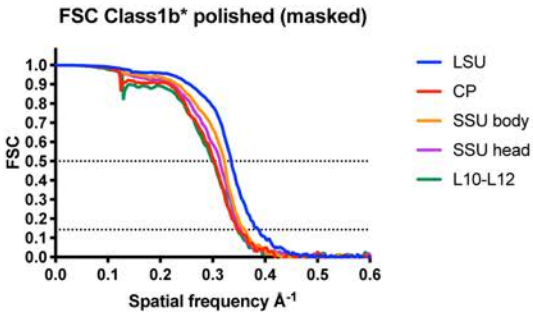

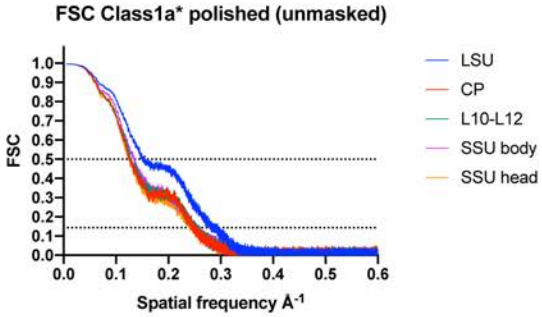

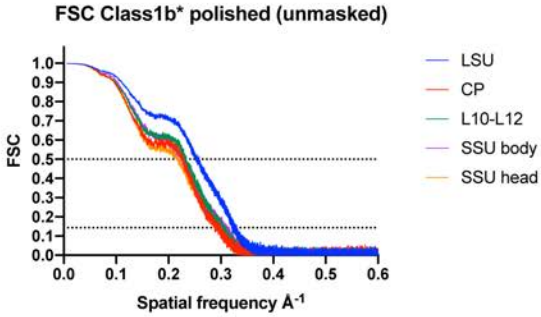

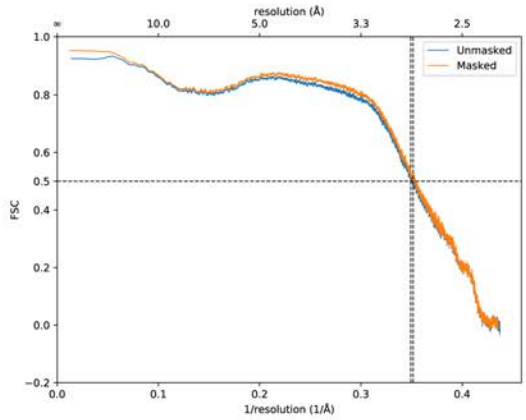

FSC Class1a* polished (model-to-map)

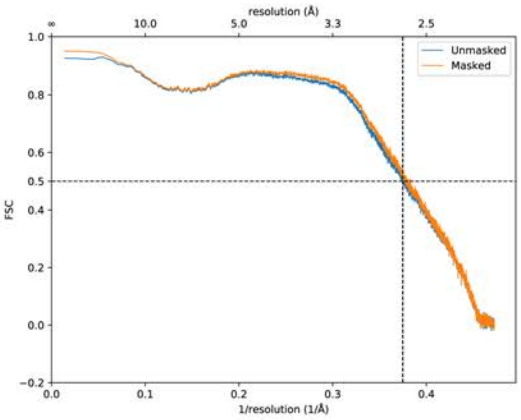

FSC Class1B* polished (model-to-map)

D

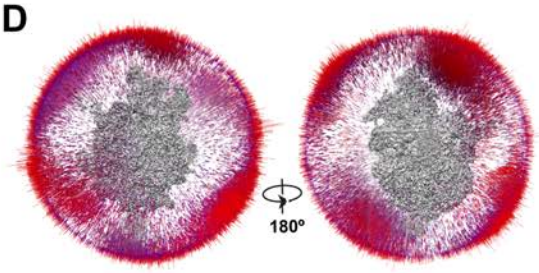

Class1a* polished

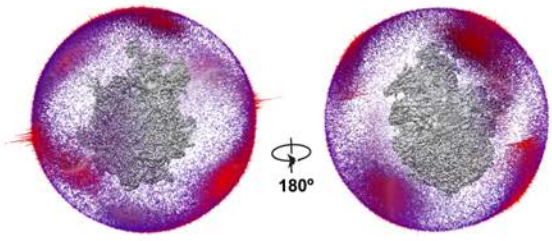

Class1b* polished

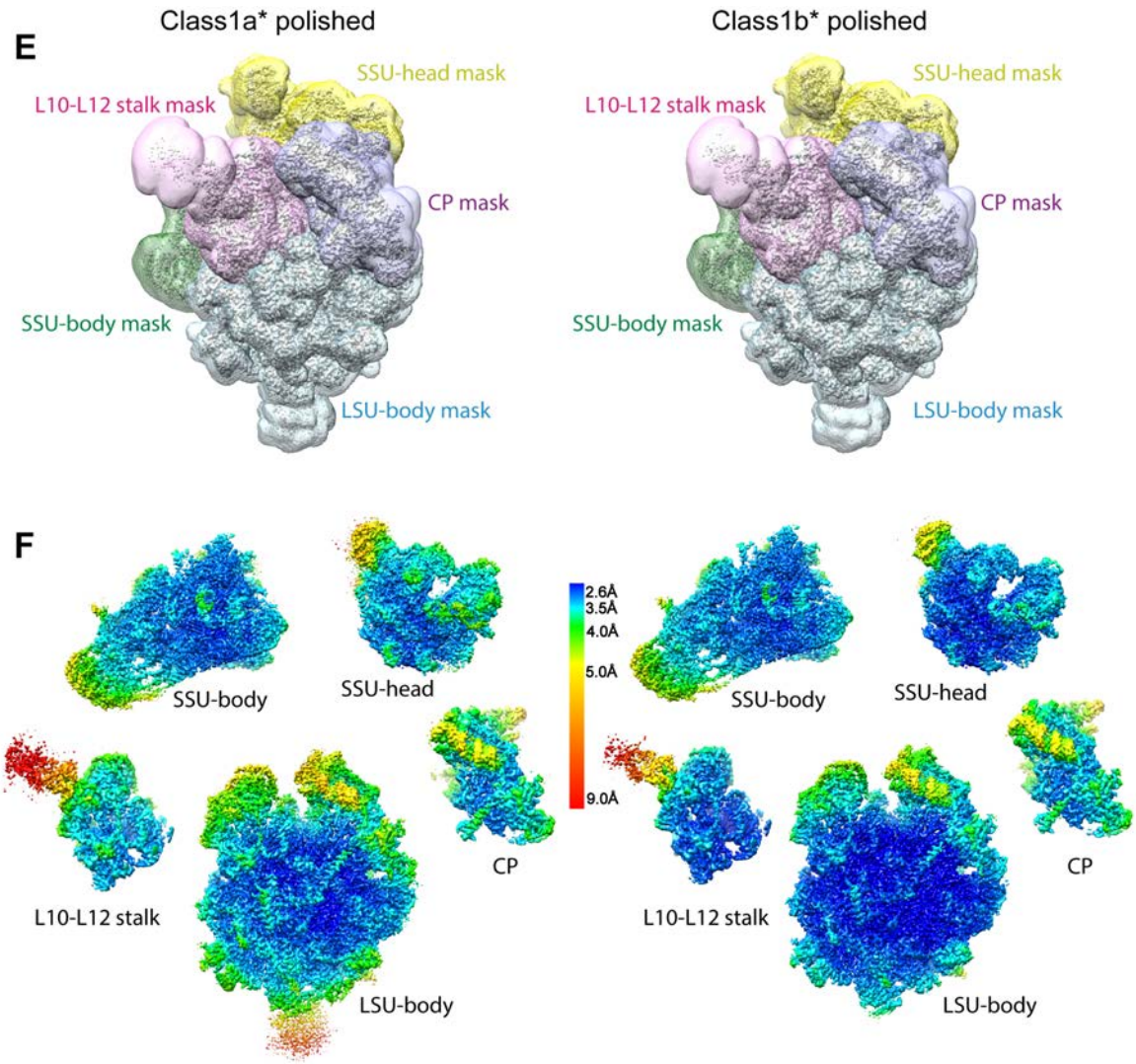

Fig. S2. Cryo-EM data collection, processing scheme and map evaluation. (A) Data sets 1-6 were collected from the native preparation, and the classification scheme revealed an additional density associated with the tunnel exit in Class 1a. **(B)** Datasets 7-8 were collected from the crosslinked preparation. Representative micrograph and 2D class averages are shown. The classification scheme resulted in OXA1L density (Class1a*) and inactive state (Class 1b*). **(C)** Fourier Shell Correlation (FSC) between two half maps (with and without applying the local masks) and the model-to-map FSC. The masked two-half-map FSCs were calculated by RELION-3.0 (*15*), while unmasked ones and the model-to-map FSCs were calculated in the PHENIX suite (*44*). **(D)** Euler angle distribution of particles from the 3D refinement using the LSU-body mask by RELION-3.0 (*15*). **(E)** Local masks used for the local-masked 3D refinement to improve the local resolution. **(F)** Local resolutions from the local-masked refinements estimation by RELION-3.0 are shown as color gradations on their corresponding masked unsharpened maps.

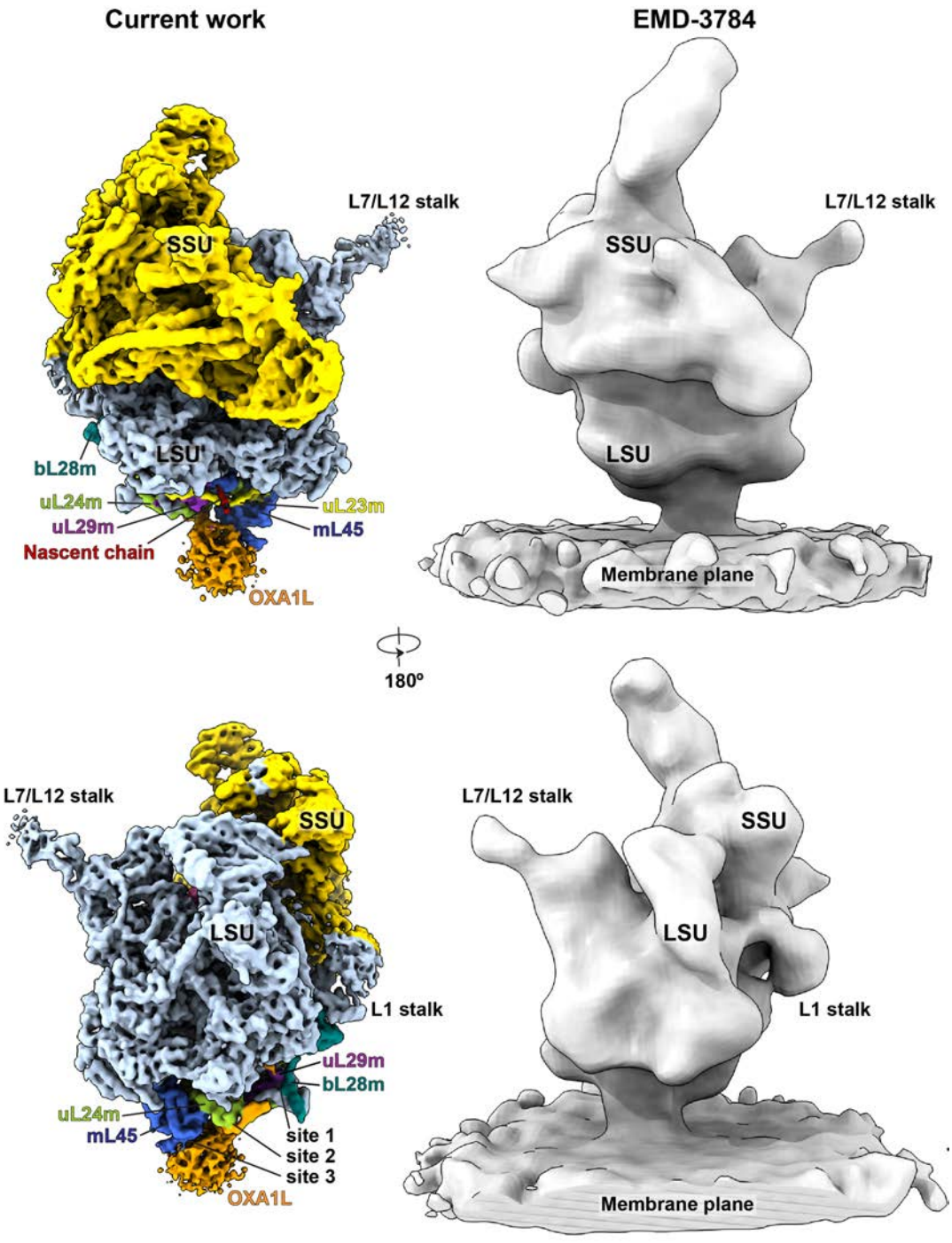

Fig. S3. Comparison of the single-particle human mitoribosome:OXA1L reconstruction with *in situ* data.

Left, single-particle cryo-EM map of the human mitoribosome:OXA1L (Class 1a*) lowpass-filtrered to 6Å for clarity. Right, cryo-ET map of *in situ* human mitoribosomes (EMD-3784 (*4*)). The density for OXA1L from single-particle corresponds to the membrane plane from tomography.

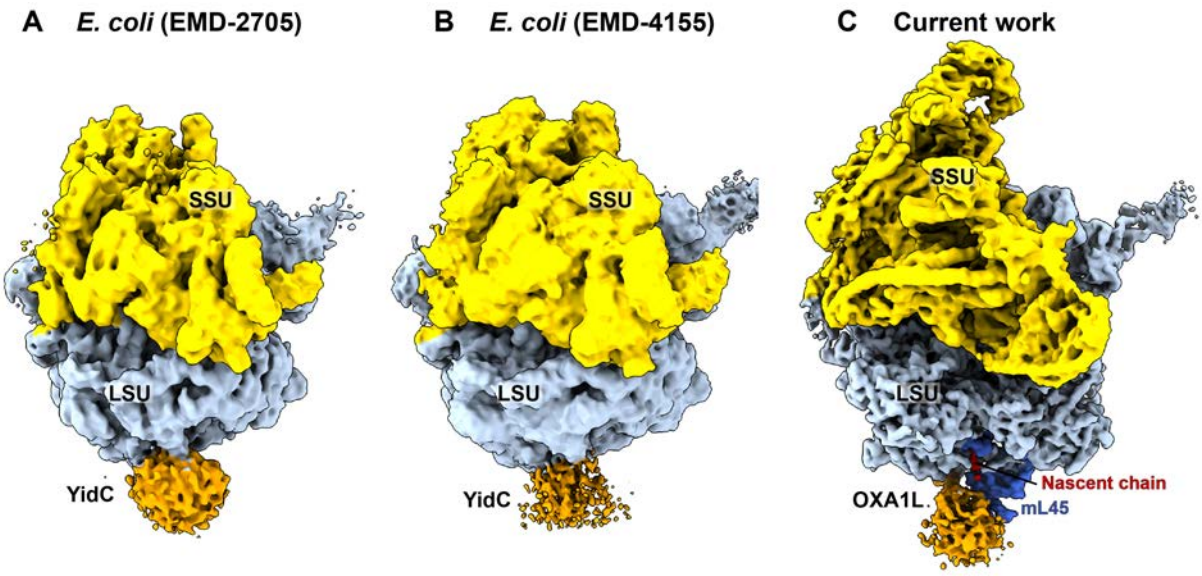

Fig. S4. Comparison of the human mitoribosome:OXA1L reconstruction with the bacterial counterparts.

(A) *Escherichia coli* ribosome:YidC complex at 8 Å resolution (EMD-2705 (*16*)) (contour level 0.2). **(B)** *Escherichia coli* ribosome:YidC, complex at 4.5 Å resolution (EMD-4155 (*17*)), lowpass-filtered to 6 Å resolution (contour level 0.004). **(C)** Human mitoribosome:OXA1L at 2.89 Å resolution (current work), lowpass-filtered to 6 Å resolution (contour level 0.004). All three maps were aligned on the LSU, and the contour level adjusted for clarity.

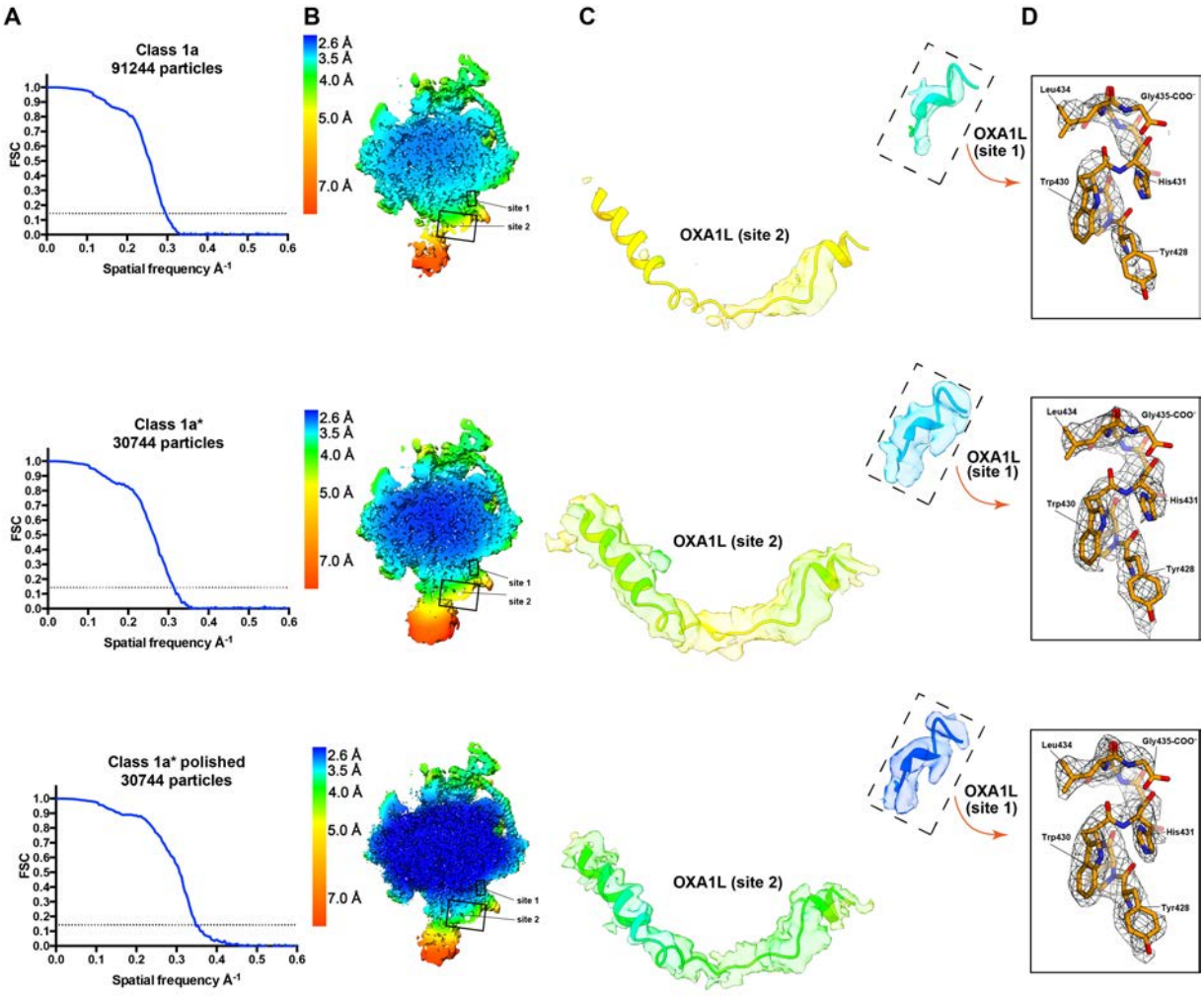

Fig. S5. Local resolution estimation and map improvement.

Top: native (Class 1a); middle: crosslinked (Class 1a*); bottom: crosslinked with particle polishing (Class 1a*). **(A)** Fourier Shell Correlation (FSC) between two half-maps. **(B)** Cut through local resolution filtered map colored according to the local resolution estimation by RELION-3.0. **(C)** OXA1L in contact site 1 and 2. The model and the unsharpened map are colored according to the local resolution estimation. **(D)** Stick model of OXA1L C-terminus (contact site 1) with sharpened map shown in mesh.

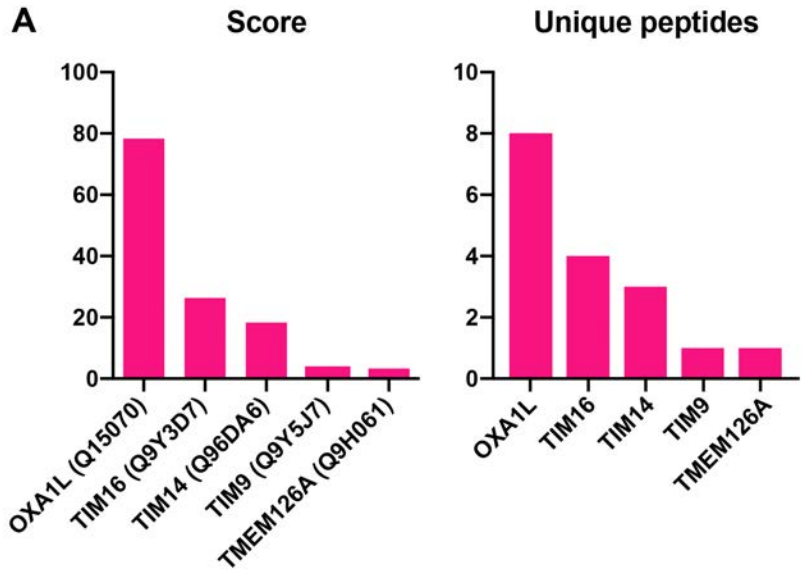

B

```
        10         20         30         40         50
MAMGLMCGRR ELLRLLQSGR RVHSVAGPSQ WLGKPLTTRL LFPVAPCCCR
        60         70         80         90        100
PHYLFLAASG PRSLSTSAIS FAEVQVQAPP VVAATPSPTA VPEVASGETA
       110        120        130        140        150
DVVQTAAEQS FAELGLGSYT PVGLIQNLLE FMHVDLGLPW WGAIAACTVF
       160        170        180        190        200
ARCLIFPLIV TGQREAARIH NHLPEIQKFS SRIREAKLAG DHIEYYKASS
       210        220        230        240        250
EMALYQKKHG IKLYKPLILP VTQAPIFISF FIALREMANL PVPSLQTGGL
       260        270        280        290        300
WWFQDLTVSD PIYILPLAVT ATMWAVLELG AETGVQSSDL QWMRNVIRMM
       310        320        330        340        350
PLITLPITMH FPTAVFMYWL SSNLFSLVQV SCLRIPAVRT VLKIPQRVVH
       360        370        380        390        400
DLDKLPPREG FLESFKKGWK NAEMTRQLRE REQRMRNQLE LAARGPLRQT
       410        420        430
FTHNPLLQPG KDNPPNIPSS SSKPKSKYPW HDTLG
```

Fig. S6. Mass spectrometry results.

(A) Mitochondrial membrane proteins identified by mass spectrometry with their accession numbers and molecular weights. The proteins are listed according to the weighted spectra from high to low: mitochondrial inner membrane protein OXA1L, mitochondrial import inner membrane translocase subunit TIM16, mitochondrial import inner membrane translocase subunit TIM14, mitochondrial import inner membrane translocase subunit TIM9, transmembrane protein TMEM126A. **(B)** The amino acid sequence for OXA1L is displayed with peptides identified by mass spectrometry shown in blue.

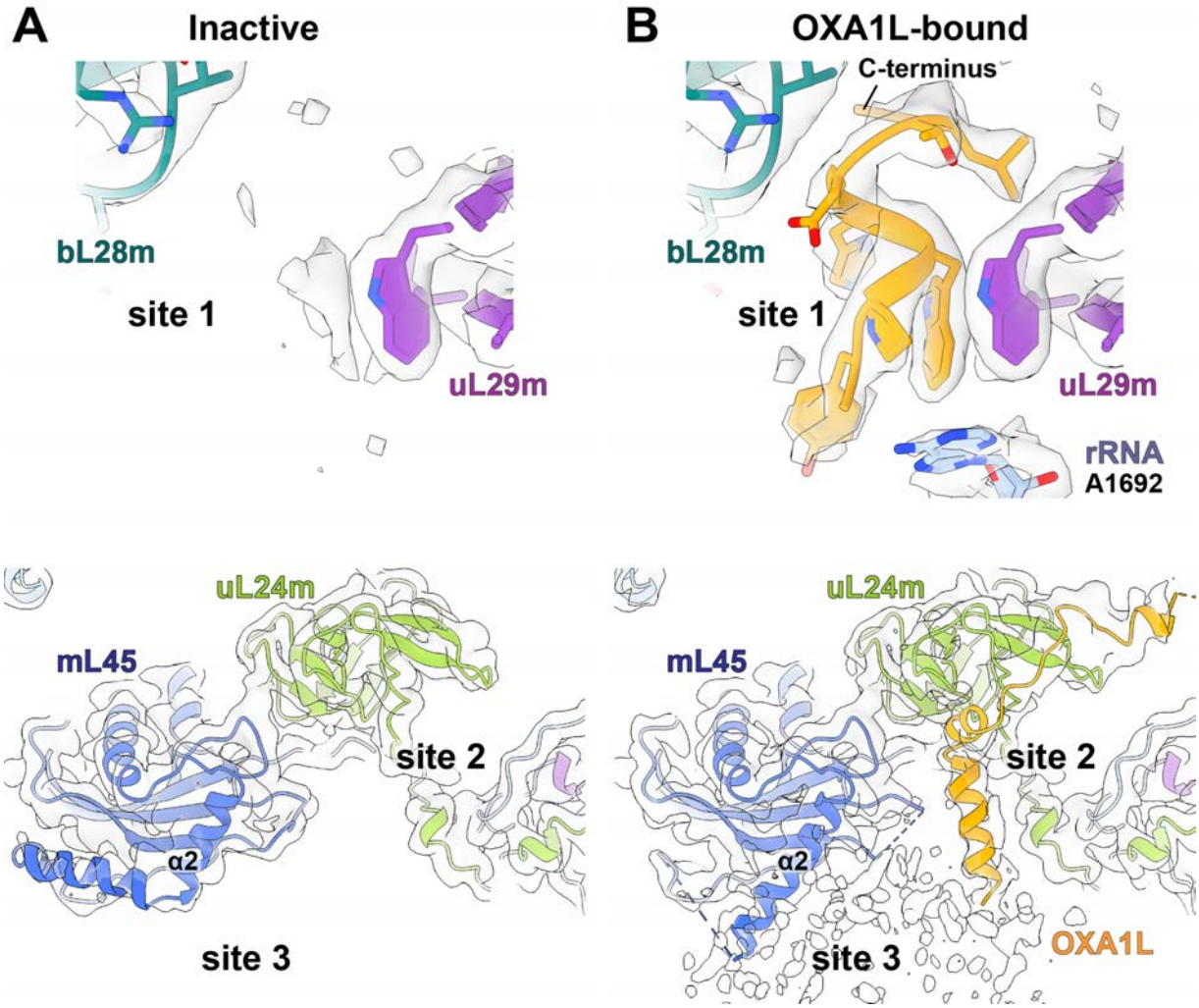

Fig. S7. Comparison of the density map at the insertase contact sites between the inactive and OXA1L-bound states.

(A) In the inactive state, only mitoribosomal density is resolved. **(B)** C-terminus of OXA1L is well resolved in site 1 (top panel), and it interacts with uL29m, bL28m, and rRNA. In sites 2 and 3 (bottom panel), OXA1L forms contacts with uL24m, and unmodeled density corresponding to the membrane region of OXA1L interacts with the extended mL45-α2. Sharpened maps are shown in the top panels, while maps lowpass-filtered to 4-Å resolution are shown in the bottom panels.

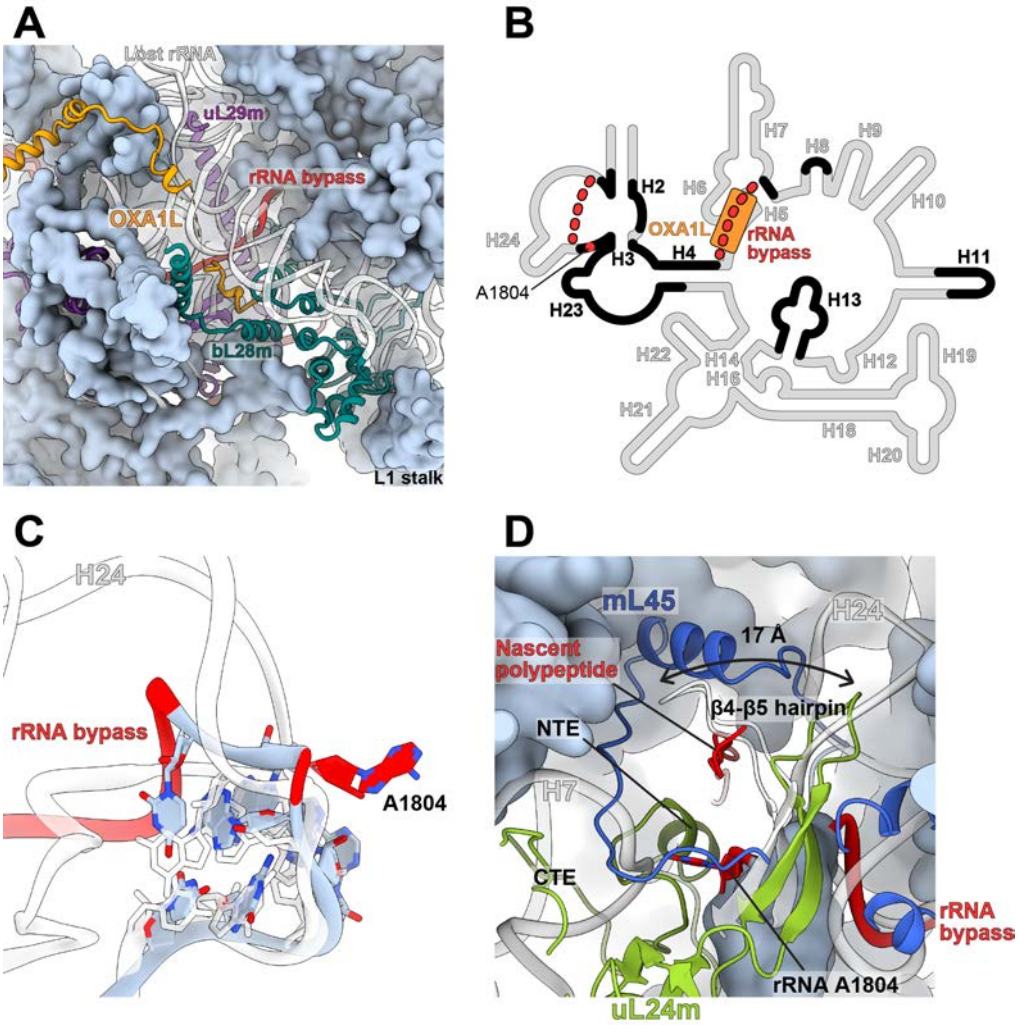

Fig. S8. Unique features of OXA1L binding pocket and the exit tunnel.
(A) OXA1L (orange) contact site 1 is formed by bL28m, uL29m, and rRNA bypass element H4-H8 (red). Other elements are shown as surface representation. The mitoribosomal proteins bL28m and uL29m are packed against each other from both sides of the OXA1L binding pocket. The rRNA bypass element connects the regions corresponding to H4 and H8, where bacterial counterpart surface-exposed regions have been excised. These rRNA deletions are represented by the superposed *E. coli* ribosome (PDB ID 4YBB (*60*)), shown as white ribbons. **(B)** Secondary structure diagram of rRNA H2-H24 shows largely deleted fragments (gray) of ~320 nucleotides, representing the most substantial reduction of rRNA domain in the mitoribosome. The retained rRNA (black) is connected via bypass elements (dashed red). The bypass H4-H8 contributes to the OXA1L binding pocket in the contact site 1. **(C)** The single-residue insertion A1804 (red) is represented through the superposition with the *E. coli* rRNA (white). **(D)** The tunnel exit region comparison with the bacterial ribosome. The rRNA helices H7 and H24 and the uL24m β4-β5 hairpin from the superposed *E. coli* ribosome are shown as white ribbon diagrams. rRNA H7 deletion is compensated by uL24m N- and C-terminal extensions (NTE and CTE), whereas rRNA H24 deletion is compensated by uL24m β4-β5 hairpin that changes the orientation (black arrow). The rRNA A1804 stabilizes mL45 folding inside the tunnel. Surface representation is shown except for the described elements.

A

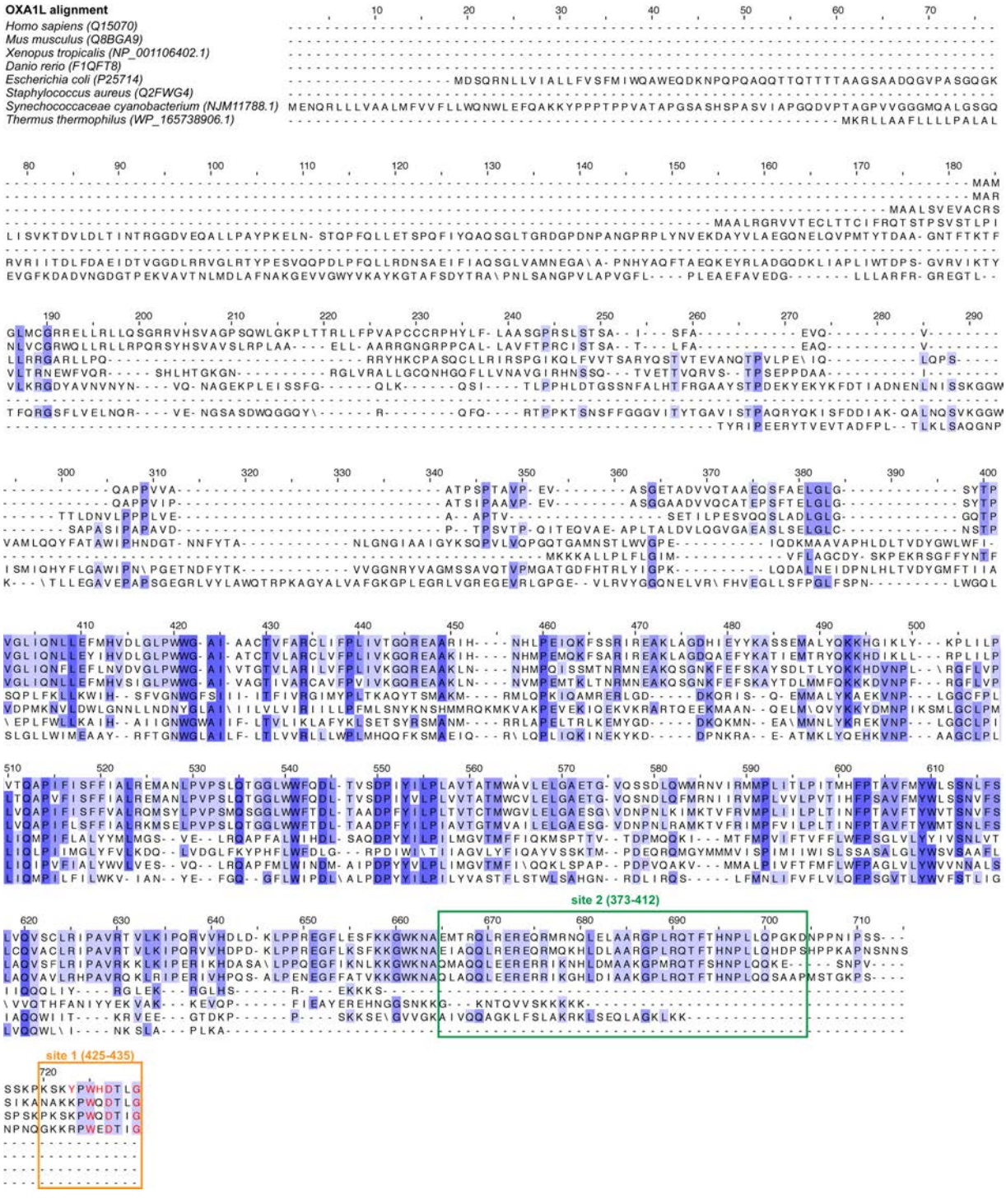
OXA1L alignment
Homo sapiens (Q15070)
Mus musculus (Q8BGA9)
Xenopus tropicalis (NP_001106402.1)
Danio rerio (F1QFT8)
Escherichia coli (P25714)
Staphylococcus aureus (Q2FWG4)
Synechococcaceae cyanobacterium (NJM11788.1)
Thermus thermophilus (WP_165738906.1)
site 2 (373-412)
site 1 (425-435)

B

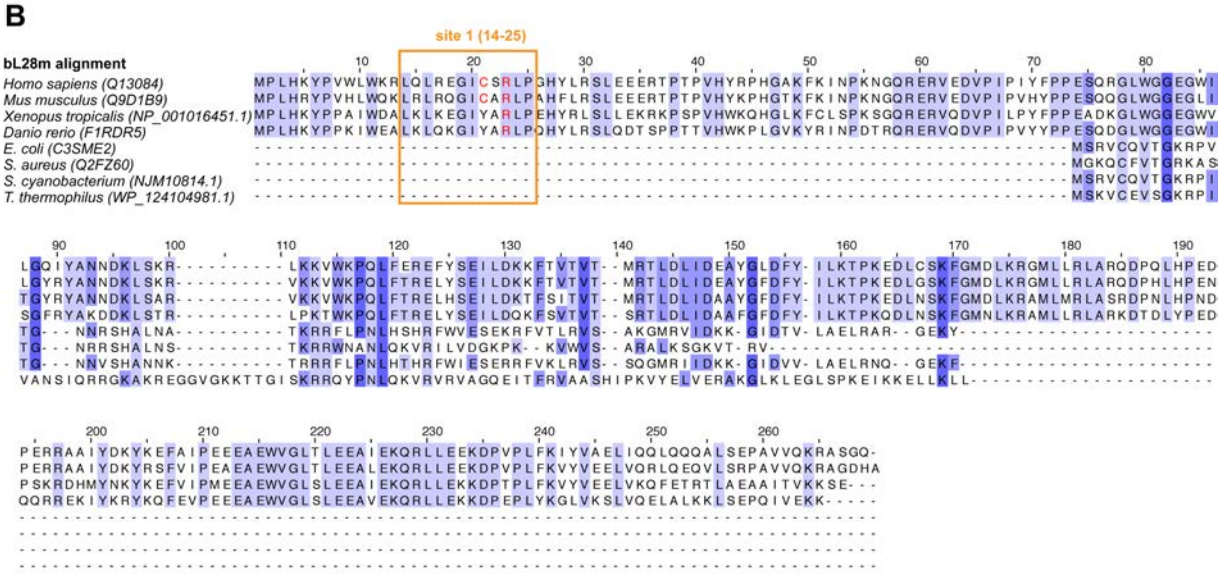
site 1 (14-25)
bL28m alignment
Homo sapiens (Q13084)
Mus musculus (Q9D1B9)
Xenopus tropicalis (NP_001016451.1)
Danio rerio (F1RDR5)
E. coli (C3SME2)
S. aureus (Q2FZ60)
S. cyanobacterium (NJM10814.1)
T. thermophilus (WP_124104981.1)

C

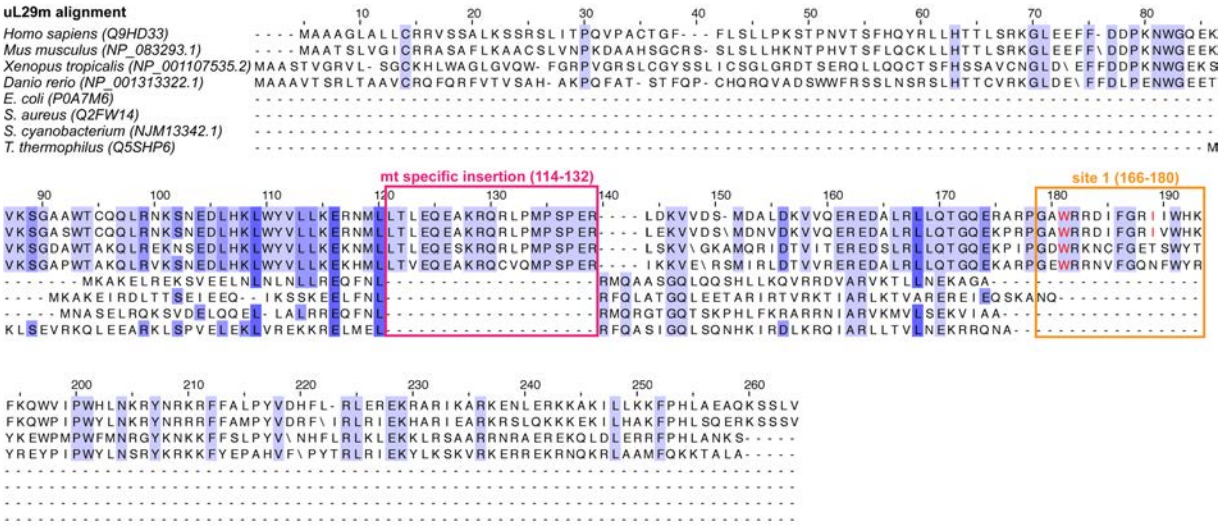
uL29m alignment
Homo sapiens (Q9HD33)
Mus musculus (NP_083293.1)
Xenopus tropicalis (NP_001107535.2)
Danio rerio (NP_001313322.1)
E. coli (P0A7M6)
S. aureus (Q2FW14)
S. cyanobacterium (NJM13342.1)
T. thermophilus (Q5SHP6)
mt specific insertion (114-132)
site 1 (166-180)

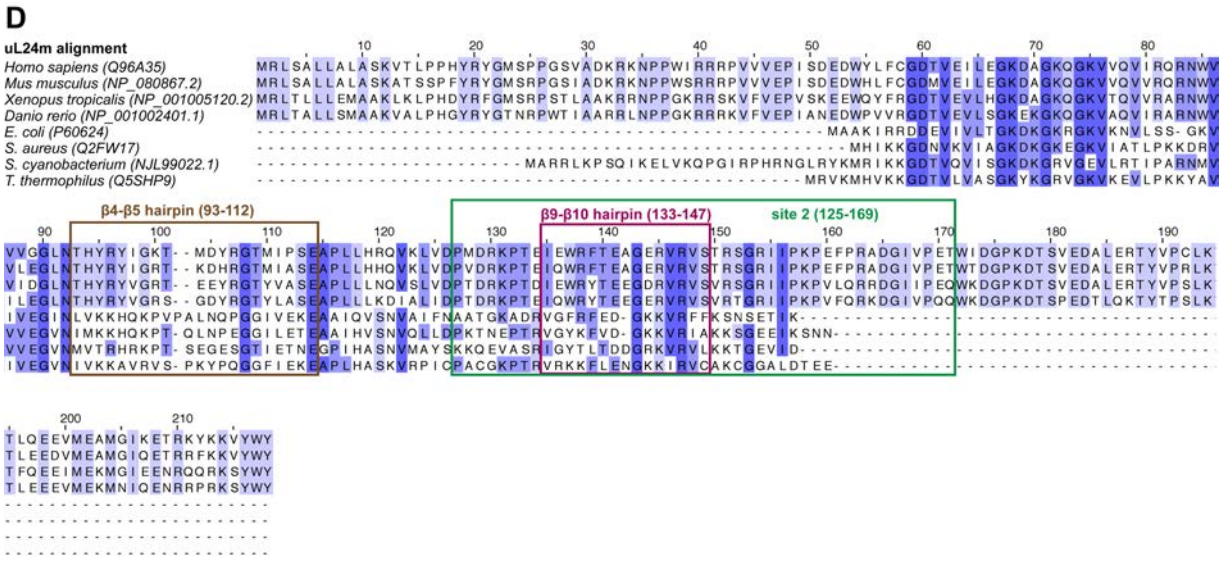

Fig. S9. Sequence alignment of the elements forming OXA1L binding sites.

(A) OXA1L alignment shows that vertebrate sequences (top four) are conserved in the contact sites 1 and 2 (framed), but not in bacterial YidC sequences (bottom four). **(B)** bL28m alignment shows that vertebrate sequence extensions are conserved in the contact site 1. **(C)** bL29m alignment shows that vertebrate sequence insertion contact site 1 are conserved. **(D)** uL24m alignment. The site 2 and the β4-β5 hairpin are indicated.

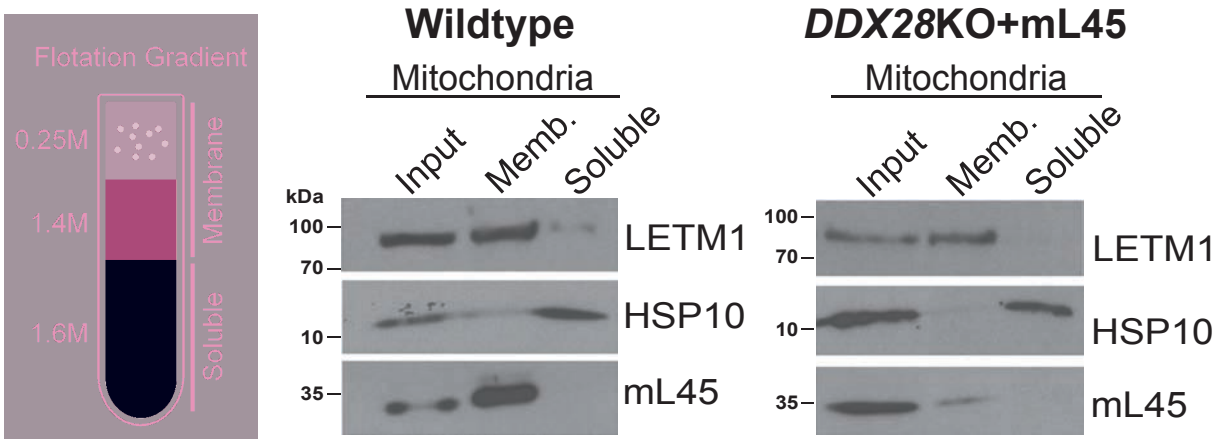

Fig. S10. Membrane association of mL45.

Mitochondria from the WT or *DDX28*-KO cells overexpressing *mL45* were sonicated, and the soluble or membrane-associated proteins were separated. Equal volumes of the membrane and soluble fractions were loaded (non-equal amount of sample is shown as Input for protein-detection control). The assay was controlled by immunoblotting against markers of the membrane-associated fraction with the membrane-integral protein LETM1, and the soluble fraction with HSP10.

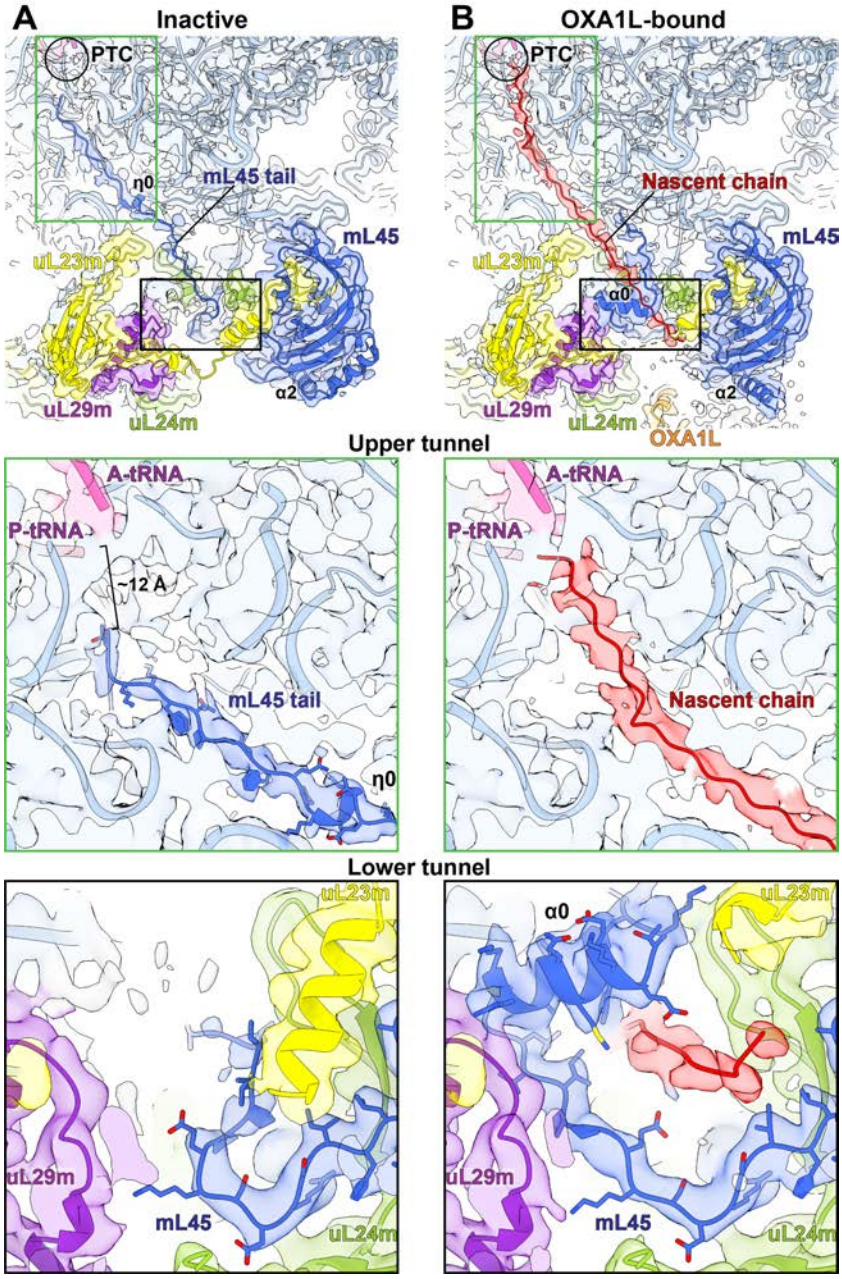

Fig. S11. Comparison of the density map in the tunnel region between the inactive and OXA1L-bound states.

(A) In the inactive state, the density for mL45 N-terminal tail (blue) occupies the upper tunnel, leaving 12-Å distance from the P-tRNA (middle panel). In the lower tunnel (bottom panel) mL45 interacts with uL23m. **(B)** In the OXA1L-bound state, a continuous density of a nascent synthesized polypeptide chain (red) extends from the P-tRNA (middle panel) throughout the tunnel towards the exit (bottom panel), where mL45 adopts a conformational change, forming contacts with uL29m that results in an arch that prevents helical formation of the nascent chain, while directing it to the membrane. Lowpass-filtered maps at 4 Å resolution are shown.

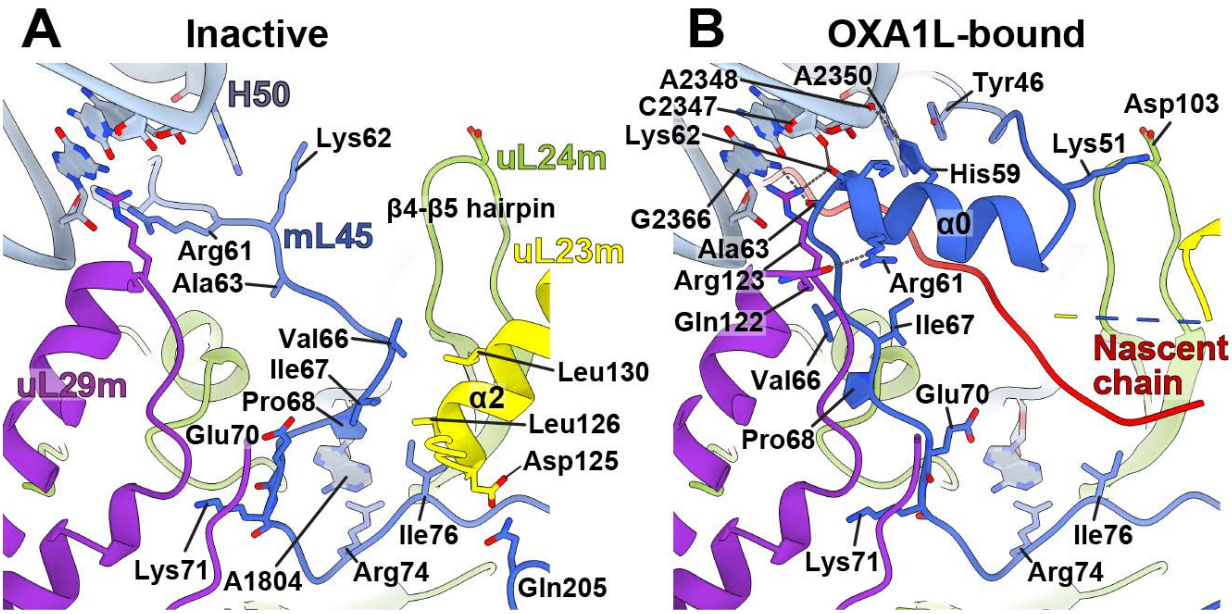

Fig. S12. The mL45 N-terminal tail interactions in tunnel.

(A) In the inactive state, the Glu70-Lys71 peptide adopts a left-handed-helix-like conformation stabilized by Pro68 forming hydrophobic interactions with rRNA A1804, mL45 Ile76, and uL23m Leu126. Val66 and Ile67 in the mL45 N-terminal tail form inter-protein hydrophobic pairs with the uL23m-α2 Leu126 and Leu130. Gln205 in the loop from mL45 Tim44-like domain interacts with Asp125 in uL23m-α2 from the opposite side. A1804 is stacked by mL45 Arg74. Positively charged residues are pointed toward the rRNA tunnel interior. **(B)** In the OXA1L-bound state, the Glu70-Lys71 peptide adopts a β-strand-like conformation, resulting in the reorientation of the upstream residues. The interactions with uL23m are broken, the mL45 tail is retracted from the tunnel and folded into α0 to form an arch inside the tunnel securing the path for nascent polypeptide (red). This folding is stabilized by the interactions with rRNA H50, uL24m and uL29m. mL45 Tyr46 is stacked on rRNA A2350 in H50. His59 sidechain hydrogen-bonds with A2348 ribose. Lys62 and Ala63 backbone carbonyls hydrogen-bond with C2347 ribose and G2366 base, respectively. The mL45 Lys51 sidechain contacts the uL24m Asp103 sidechain from the β4-β5 hairpin. The mL45 Arg61 sidechain and Lys62 backbone carbonyl hydrogen-bond with the uL29m Gln122 backbone carbonyl and Arg123 sidechain, respectively.

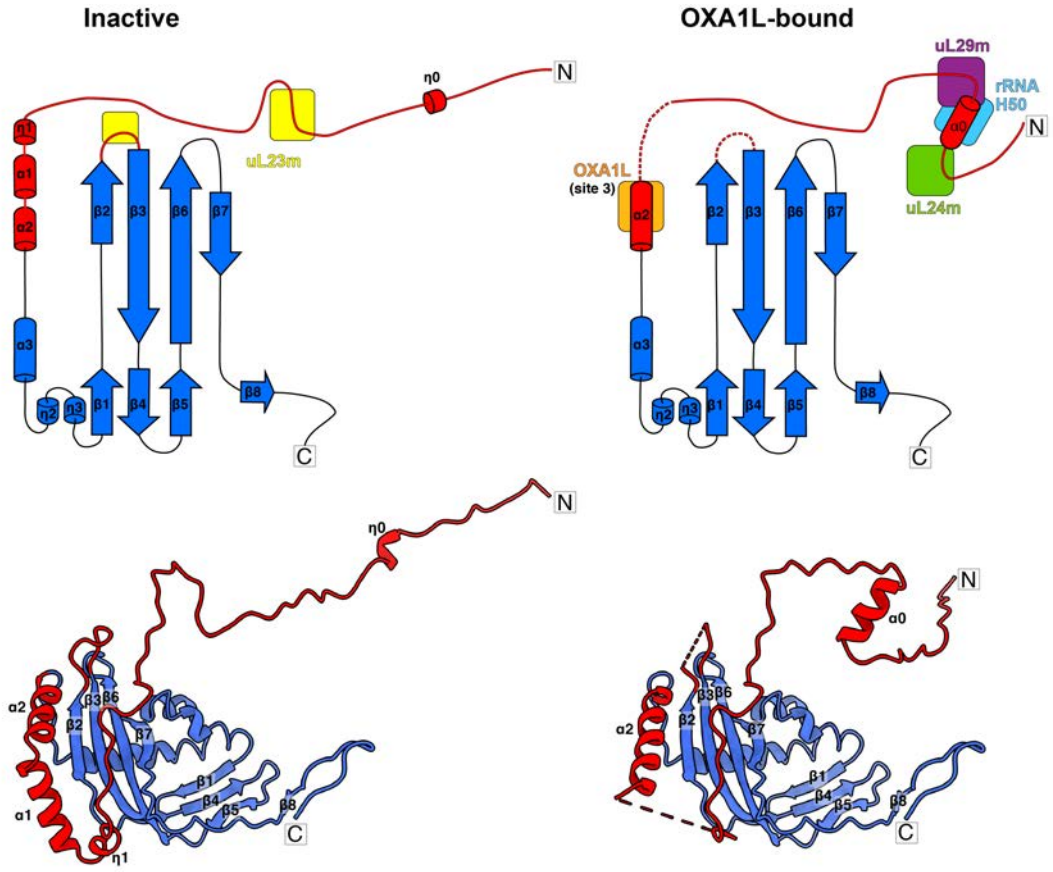

Fig. S13. Conformational changes in mL45 that lead to the gating mechanism.

In the inactive state (left), mL45 adopts the extended conformation that is stabilized by uL23m-α2, and together blocks the path. In the OXA1L-bound state (right), mL45-α0 is folded inside the tunnel that is stabilized by uL24m, uL29m and rRNA H50. OXA1L binds to the extended mL45-α2. The regions of mL45 that undergo conformational changes are shown in red.

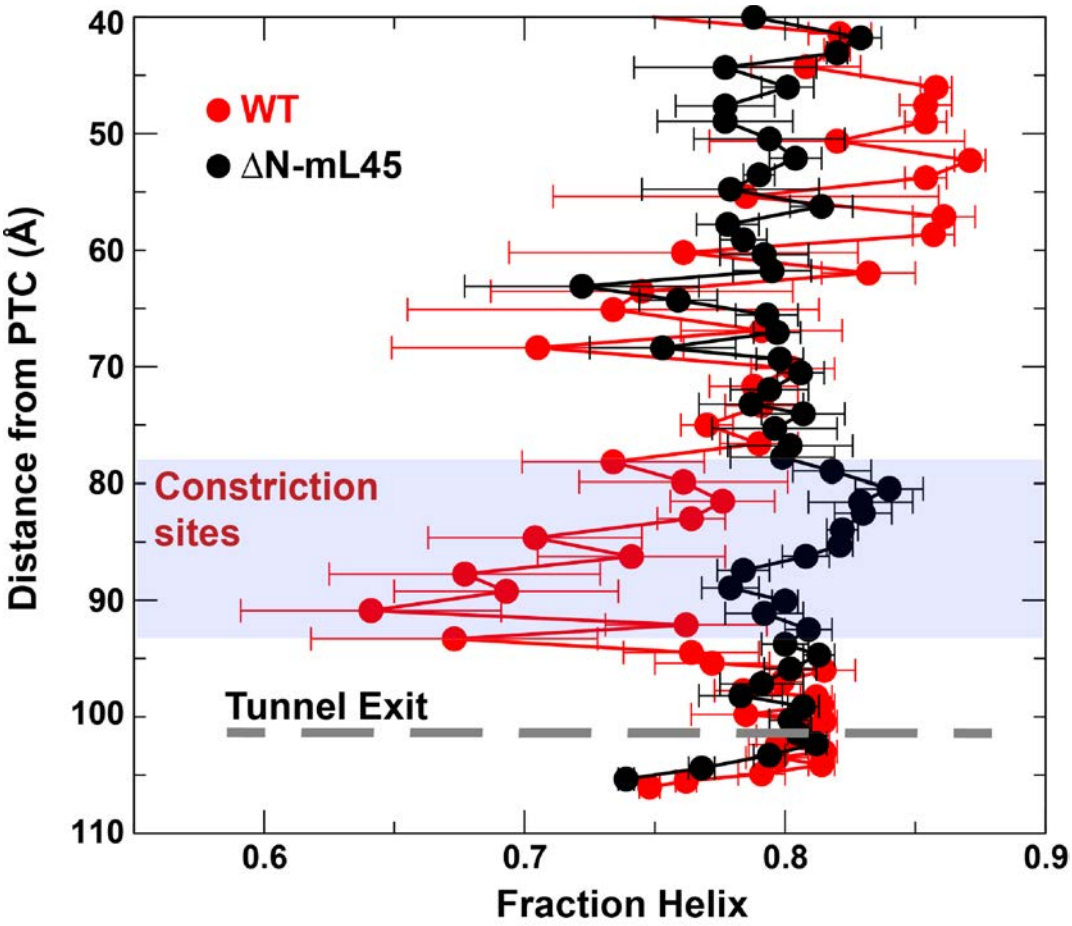

Fig. S14. Coarse-grained molecular dynamics simulations of a nascent chain folding with WT and Δ*N-mL45* mitoribosomes.

Initial structures were taken from the all-atom model of the OXA1L-bound complex, and residues added to the N-terminus of the nascent chain. Each protein residue was represented by a single bead centered on the C_α carbon atom, and the interactions were then calculated with a coarse-grained energy function accounting for contacts favoring helix formation for WT (red) and Δ*N-mL45* mitoribosomes (black) (see Methods). The results are plotted in a curve (each residue of the nascent chain represented by a sphere) as a function of the distance from the PTC and an indicator of a helix formation probability termed "Fraction Helix". The lowest values for the WT are found in the tunnel region 78-93 Å from the PTC that corresponds to the position of the constriction sites (see Fig. 4D). In the respective simulation for the Δ*N-mL45* mitoribosomes, the nascent chain residues in the same region are more likely to fold into helix, relative to the WT mitoribosomes, supporting the assignments of the constriction sites.

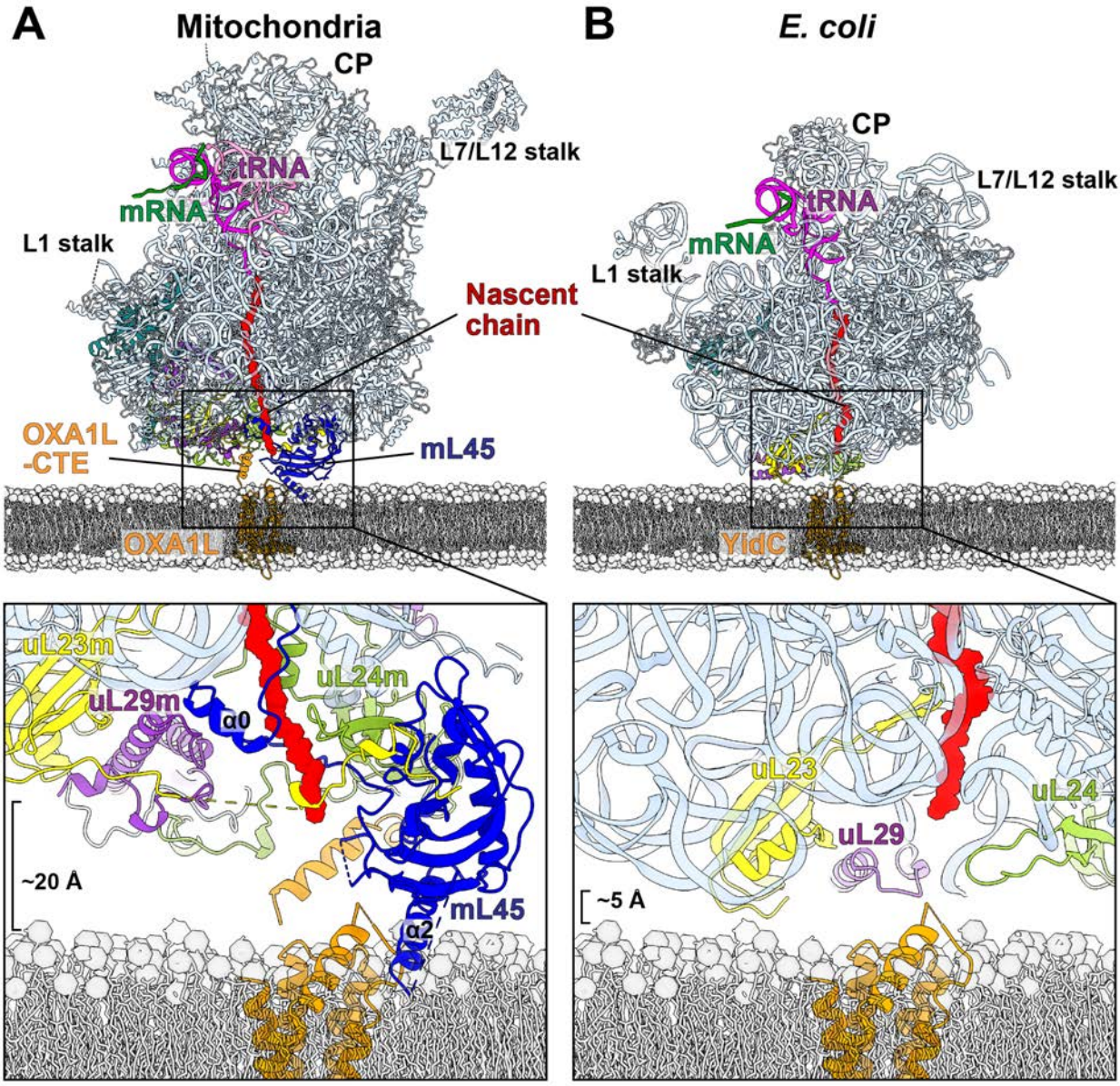

Fig. S15. The positioning of the tunnel exit in relation to the membrane.

(A) In mitochondria, mL45-OXA1L interactions increase the distance between the mitoribosomal tunnel exit and the membrane insertion point up to ~20 Å (measured from the mainchain of the conserved part of uL24m, see Methods). The gap would allow a solvent-exposed nascent polypeptide (red) to be accessible to specific maturation factors and chaperones before the membrane insertion. The folding of the membrane-distal mL45-α0 prevents an α-helical formation of membrane proteins within the tunnel. SSU is not shown for clarity. **(B)** The corresponding ribosome-insertase interactions in *E. coli* (EMD-4155 (*17*)) imply closer association of the tunnel exit with the insertase, and a formation of α-helical membrane domains are more likely to occur within the tunnel.

Table S1. Data collection, processing, model refinement and validation statistics.

	Class1a* polished (PDB ID: 6ZM5) (EMD-11278)	Class1b* polished (PDB ID: 6ZM6) (EMD-11279)
Data collection and Processing		
Microscope	Titan Krios	Titan Krios
Voltage (kV)	300	300
Camera	K2 Summit	K2 Summit
Magnification	165,000	165,000
Pixel size at detector (Å/pixel)	0.83	0.83
Total electron exposure (e^{-}/Å^2)	29–32	29–32
Exposure rate (e^{-}/pixel/sec)	5.0–5.7	5.0–5.7
Number of frames	20	20
Defocus range (μm)	−0.2 to −3.6	−0.2 to −3.6
Automation software	EPU	EPU
Energy filter slit width (V)	20	20
Micrographs collected (no.)	19,667	19,667
Micrographs used (no.)	18,162	18,162
Total extracted particles (no.)	1,156,223	1,156,223
Refined particles (no.)	241,399	241,399
Final particles (no.)	30,744	93,615
Point group	C_1	C_1
Resolution (global, Å) FSC 0.50 (unmasked) (LSU-body/ CP/ L10-L12-stalk/ SSU-body/ SSU-head)	6.65/ 8.03/ 7.86/ 7.44/ 8.00	3.90/ 4.47/ 4.37/ 4.45/ 4.66
Resolution (global, Å) FSC 0.50 (masked) (LSU-body/ CP/ L10-L12-stalk/ SSU-body/ SSU-head)	3.25/ 3.93/ 3.97/ 3.59/ 3.70	2.99/ 3.30/ 3.34/ 3.11/ 3.20
Resolution (global, Å) FSC 0.143 (unmasked) (LSU-body/ CP/ L10-L12-stalk/ SSU-body/ SSU-head)	3.59/ 4.11/ 4.09/ 4.06/ 4.18	3.10/ 3.48/ 3.37/ 3.37/ 3.45
Resolution (global, Å) FSC 0.143 (masked) (LSU-body/ CP/ L10-L12-stalk/ SSU-body/ SSU-head)	2.89/ 3.20/ 3.16/ 3.03/ 3.07	2.59/ 2.89/ 2.89/ 2.78/ 2.84
Map-sharpening *B* factor [Å^2] (LSU-body/ CP/ L10-L12-stalk/ SSU-body/ SSU-head)	−37/ −65/ −64/ −45/ −51	−39/ −54/ −61/ −55/ −49
Map sharpening methods	Guinier plot	Guinier plot
Model composition		
Total atoms (non-hydrogen/ hydrogen)	177,135/ 149,906	176,757/ 149,543
Chains (RNA/ protein)	6/ 88	6/ 86
RNA residues	2,717	2,714
Protein residues (non-modified/ modified)	14,564/ 6	14,516/ 6
Metal ions (Mg^{2+}/ K^{+}/ Zn^{2+})	189/ 44/ 3	189/ 44/ 3
Ligands (ATP/ GTP/ 2Fe-2S)	1/ 1/ 3	1/ 1/ 3

Waters	470	470
Model Refinement		
Refinement method	Real space	Real space
Model-Map CC (CC_{mask}/ CC_{box}/ CC_{peaks}/ CC_{volume})	0.85/ 0.81/ 0.77/ 0.83	0.86/ 0.83/ 0.79/ 0.82
Average *B* factor (Å^2) (RNA/ protein/ metal ion and ligand/ water)	42/ 45/ 37/ 21	44/ 44/ 40/ 24
R.m.s. deviations		
Bond lengths (Å)	0.003	0.003
Bond angles (°)	0.42	0.42
Validation		
MolProbity score	1.02	1.00
CaBLAM outliers (%)	0.79	0.77
Clash score	2.4	2.2
Rotamer outliers (%)	0.05	0.06
C_β deviations	0	0
EMRinger score	4.27	4.72
Ramachandran plot (%) (Favored/ allowed/ disallowed)	98.84/ 1.16/ 0.01	98.85/ 1.14/ 0.01
Accession ID		
EMDB ID (LSU-body/ CP/ L10-L12-stalk/ SSU-body/ SSU-head)	EMD-11278/ EMD-11280/ EMD-11281/ EMD-11282/ EMD-11283	EMD-11279/ EMD-11284/ EMD-11285/ EMD-11286/ EMD-11287

Table S2. Modeled RNA and proteins in mtLSU.

Name	Uniprot ID	Chain ID	Modeled residues	Predicted mature RNA/protein	Notes
16S rRNA	NR_137295.1 (Ref_seq) NC_012920.1 (Ref_seq mt-gDNA)	A	1671–2759, 2787–3231	1671–3229	
$tRNA^{Val}$		B	1602–1673 (with CCA end)	1602–1673 (with CCA end)	The CCA end is modeled.
uL2m	Q5T653	D	61–298	61–305	Metal ion coordinated by Asp132 and Arg135.
uL3m	P09001	E	44–348	41–348	Cis peptide at Pro316.
uL4m	Q9BYD3	F	44–295	1–311	Cis peptides at Pro155 and Pro294.
uL9m	Q9BYD2	H	53–149	53–267	
uL10m	Q7Z7H8	I	29–240	29–261	Cys64 coordinates a 2Fe-2S cluster with mL66 Cys70, Cys73 and Cys108.
uL11m	Q9Y3B7	J	18–192	?–192	
uL13m	Q9BYD1	K	2–178	2–178	N-acetylated Ser2.
uL14m	Q6P1L8	L	31–145	31–145	
uL15m	Q9P015	M	6–296	22–296	
uL16m	Q9NX20	N	30–251	30–251	
bL17m	Q9NRX2	O	9–162	9–175	
uL18m	Q9H0U6	P	37–180	?–180	Cis peptide at Pro73.
bL19m	P49406	Q	55–292	?–292	Bridging the LSU core to the SSU tail. Cis peptide at Pro227.
bL20m	Q9BYC9	R	10–149	10–149	
bL21m	Q7Z2W9	S	45–205	40–205	Cis peptide at Pro147.
uL22m	Q9NWU5	T	41–206	41–206	
uL23m	Q16540	U	2–153	1–153	N-acetylated Ala2. The helix 125–135 is disordered when there is a nascent polypeptide.
uL24m	Q96A35	V	12–216	?–216	
bL27m	Q9P0M9	W	33–148	31–148	The N-terminal region interacts with the P-site tRNA.

bL28m	Q13084	X	2–245	56–256	Interacts to the OXA1L C-terminus.
uL29m	Q9HD33	Y	63–243	?–250	Interacts to the OXA1L C-terminus.
uL30m	Q8TCC3	Z	35–56	35–161	
bL32m	Q9BYC8	0	79–188	?–188	Zn^{2+} coordination (Cys110, Cys113, Cys123, Cys126).
bL33m	O75394	1	11–65	9–65	
bL34m	Q9BQ48	2	47–92	47–92	
bL35m	Q9NZE8	3	94–188	?–188	
bL36m	Q9P0J6	4	66–103	?–103	Zn^{2+} coordination (Cys76, Cys79, Cys92, His98).
mL37	Q9BZE1	5	30–423	30–423	
mL38	Q96DV4	6	27–380	27–380	Cis peptide at Pro289.
mL39	Q9NYK5	7	34–327	1–338	Cis peptide at Pro288.
mL40	Q9NQ50	8	47–203	47–206	The N-terminal region interacts to A- and P-site tRNAs. Cis peptide at Pro170.
mL41	Q8IXM3	9	14–137	14–137	Cis peptide at Pro132.
mL42	Q9Y6G3	a	35–79, 88–142	33–142	
mL43	Q8N983	b	2–151	?–215	N-acetylated Thr2.
mL44	Q9H9J2	c	31–110, 115–320	31–332	Cis peptide at Pro185.
mL45	Q9BRJ2	d	37–295	?–306	
mL46	Q9H2W6	e	42–101, 112–279	?–279	
mL48	Q96GC5	f	48–68, 80–212	29–212	
mL49	Q13405	g	33–166	1–166	Cis peptides at Pro67 and Pro78.
mL50	Q8N5N7	h	49–158	1–158	
mL51	Q4U2R6	i	32–128	32–128	
mL52	Q86TS9	j	23–116	24–123	
mL53	Q96EL3	k	2–102	?–112	N-acetylated Ala2.
mL54	Q6P161	l	55–137	15–138	
bL31	Q7Z7F7	m	34–126	34–128	Bridging the mtLSU CP to the mtSSU head.
mL63	Q9BQC6	o	9–102	1–102	
mL62	Q14197	p	38–64, 69–88, 93–195	30–206	
mL64	Q8TAE8	q	25–185	1–222	The C-terminal region contacts the P-site tRNA.

mL66	Q9NVS2	r	35–196	35–196	Cys70, Cys73 and Cys108 coordinate a 2Fe-2S cluster with uL10m Cys64.
mL65	Q9NP92	s	39–125, 135–433	1–439	Cis peptide at Pro272.
bL12m	P52815	t1	46–91	46–198	The first copy.
bL12m	P52815	t2, t3	60–91	46–198	The second and third copies.
bL12m	P52815	t4, t5, t6	61–91	46–198	The fourth to sixth copies.

Table S3. Modeled RNA and proteins in mtSSU.

Name	Uniprot ID	Chain ID	Modeled residues	Predicted mature RNA/protein	Notes
12S rRNA	NR_137294.1 (Ref_seq) NC_012920.1 (Ref_seq mt-gDNA)	AA	649–1602	648–1601	A750G and A1438G variant.
bS1m	Q9Y2Q9	AW	76–175	72–187	
uS2m	Q9Y399	AB	53–277	1–296	Asp224, Asp240, Asp241 and His93 seem to coordinate an Mg^{2+} ion instead of a Zn^{2+}.
uS3m	Q96EL2	AC	36–167	36–167	
uS5m	P82675	AD	88–430	1–430	
bS6m	P82932	AE	2–123	1–125	Cys105 participates in a 2Fe-2S cluster coordination with bS18m.
uS7m	Q9Y2R9	AF	35–242	38–242	
uS9m	P82933	AG	68–176, 194–396	1–396	
uS10m	P82664	AH	50–189	1–201	
uS11m	P82912	AI	58–194	1–194	Possible isoaspartate Asn184.
uS12m	O15235	AJ	31–138	30–138	Cis peptide at Pro73.
uS14m	O60783	AK	28–128	1–128	
uS15m	P82914	AL	63–236	58–257	
bS16m	Q9Y3D3	AM	10–128	35–137	Cys26 participates in a 2Fe-2S cluster coordination with mS25.
uS17m	Q9Y2R5	AN	4–113	21–130	
bS18m (bS18c)	Q9Y3D5	AP	46–142	1–142	Cys65, Cys68 and Cys100 coordinate a 2Fe-2S cluster with bS6m Cys105.
bS21m	P82921	AQ	2–87	1–87	N-acetylated Ala2. Cys50Arg variant.
mS22	P82650	AR	64–358	1–360	
mS23	Q9Y3D9	AS	2–136	2–190	
mS25	P82663	AT	2–169	1–173	Cys139, Cys141 and Cys149 coordinate a 2Fe-2S cluster with bS16m Cys26.
mS26	Q9BYN8	AU	27–202	28–205	
mS27	Q92552	AV	29–293, 311–407	37–414	

mS29	P51398	AX	47–398	22–398	GDP in the previous reports seems to be ATP with an Mg^{2+} ion. Another nucleotide binds next to Tyr173, which is GTP or GDP. Cis peptide at Pro339.
mS31	Q92665	AY	247–395	66–395	Cis peptide at Pro314.
mS33	Q9Y291	AZ	3–102	2–106	
mS34	P82930	A0	4–218	1–218	
mS35	P82673	A1	48–323	?–323	
mS37	Q96BP2	A2	2–118	1–118	N-acetylated Ala2. Potential disulfide bonds of Cys45-Cys76 and Cys55-Cys66.
mS38	Q9NWT8	A3	128–197	1–199	
mS39	Q96EY7	A4	55–207, 235–666	38–689	Cis peptides at Pro135 and Pro483.
mS40 (bS18b)	Q9Y676	AO	45–239	36–258	Zn^{2+} coordination (Cys94, Cys105, Cys108, Cys143).

Table S4. Additional models of ligands and OXA1L.

Name	Uniprot ID	Chain ID	Modeled residues	Predicted mature RNA/protein	Notes
OXA1L	Q15070	u	373–407, 426–435	?–435	
Nascent polypeptide		v	32 residues	–	Poly-alanine chain was placed and connected to the P-site tRNA.
A-site tRNA	–	w	1–76	1–76	Each residue was assigned as either A, U, G, or C, based on the density and conservation.
P-site tRNA	–	x	1–15, 21–76	1–76	Each residue was assigned as either A, U, G, or C, based on the density and conservation.
mRNA	–	y	19 residues		Each residue was assigned as either A, U, G, or C, based on the density.

Table S5. List of antibodies used in this study.

TARGET PROTEIN	COMPANY	CAT #	RRID	NOTES
ATP5A	Abcam	ab14748	AB_301447	
β-ACTIN	Proteintech	60008	AB_2289225	
bL12m (MRPL12)	Abcam	ab154961		
bS18m (MRPS18C)	Sigma	HPA050404	AB_2681115	
COX2	Abcam	ab110258	AB_10887758	
MTG1 (GTPBP7)	Sigma	HPA037827	AB_10670959	
HSPE1 (heat shock 10kDa protein 1)	LSBio	LS-C179966		
LETM1	Abcam	ab96237	AB_10678973	
mL45 (MRPL45)	Thermo	PA5-54784	AB_2644156	WB and Co-IP
mL45 (MRPL45)	abcam	ab113786	AB_10859496	WB only
mS27 (MRPS27)	Proteintech	17280-1-AP	AB_2180510	
NDUFA9	Proteintech	20312-1-AP	AB_10694678	
OXA1L	Proteintech	21055	AB_10695769	
SDHA CII 70kDa subunit	Abcam	ab14715	AB_301433	
uL14 (MRPL14)	Abcam	ab138281		
UQCRC2 (CORE2)	Abcam	ab14745	AB_2213640	
2° Ab-Mouse	Rockland Immunochemicals	610-103-121	AB_218457	
2° Ab-Rabbit	Rockland Immunochemicals	611-1302	AB_219720	